CUT FINITE ELEMENT METHODS FOR PARTIAL DIFFERENTIAL EQUATIONS ON EMBEDDED MANIFOLDS OF ARBITRARY CODIMENSIONS

ERIK BURMAN, PETER HANSBO, MATS G. LARSON, AND ANDRÉ MASSING

Abstract. We develop a theoretical framework for the analysis of stabilized cut finite element methods for the Laplace-Beltrami operator on a manifold embedded in $\mathbb{R}^d$ of arbitrary codimension. The method is based on using continuous piecewise linears on a background mesh in the embedding space for approximation together with a stabilizing form that ensures that the resulting problem is stable. The discrete manifold is represented using a triangulation which does not match the background mesh and does not need to be shape-regular, which includes level set descriptions of codimension one manifolds and the non-matching embedding of independently triangulated manifolds as special cases. We identify abstract key assumptions on the stabilizing form which allow us to prove a bound on the condition number of the stiffness matrix and optimal order a priori estimates. The key assumptions are verified for three different realizations of the stabilizing form including a novel stabilization approach based on penalizing the surface normal gradient on the background mesh. Finally, we present numerical results illustrating our results for a curve and a surface embedded in $\mathbb{R}^3$.

1. Introduction

In this paper, we develop a unified analysis for stabilized cut finite element methods for the Laplace-Beltrami problem

$$-\Delta_\Gamma u = f \quad \text{on } \Gamma \tag{1.1}$$

posed on compact, smooth d-dimensional manifolds embedded in $\mathbb{R}^k$ without boundary. Here, $f \in L^2(\Gamma)$ is assumed to satisfy $\int_\Gamma f = 0$ to guarantee the unique solvability of problem (1.1).

The cut finite element method is a recently developed, general unfitted finite element technique to facilitate the numerical solution of partial differential equations (PDEs) on complex geometries [3], including PDEs on surfaces embedded in $\mathbb{R}^3$ [28]. The method uses restrictions of standard continuous piecewise linear finite elements defined on a partition of the embedding space into tetrahedra, the so called background mesh, to a piecewise linear approximation of the exact surface. The discrete surface is allowed to cut through the background mesh in an arbitrary fashion. The set of elements in the background mesh intersected by the discrete surface forms the so called active mesh which supports the piecewise linears involved in the computation. This approach leads to a potentially ill posed stiffness matrix and therefore either preconditioning [27] or stabilization [4, 7] is required. In [4], a consistent stabilization term was introduced that provides control of the jump in the normal gradient on each of the interior faces in the active mesh. In constrast, the stabilization proposed and analyzed in [7] provides control over the full gradient on the elements in the active mesh and is only weakly consistent. Optimal order a priori error estimates and condition number estimates are established for both types of stabilization in [4, 7]. Further developments in this area include convection problems on surfaces [5, 29], Darcy flows on surfaces [24], cut discontinuous Galerkin methods [6], higher order discretizations [17, 18], adaptive methods based on a posteriori error estimates [9, 13], coupled surface bulk problems [8, 21], and time dependent problems [23, 27, 30]. See also the review article [3] on cut finite element

Date: April 13, 2018.

2010 *Mathematics Subject Classification.* Primary 65N30; Secondary 65N85, 58J05.

Key words and phrases. Surface PDE, Laplace-Beltrami operator, cut finite element method, stabilization, condition number, a priori error estimates, arbitrary codimension.

methods and references therein, and [15] for general background on finite element methods for surface partial differential equations.

1.1. **Novel contributions.** In this contribution we develop a stabilized cut finite element framework for the Laplace-Beltrami operator on a d-dimensional manifold without boundary embedded in $\mathbb{R}^k$, with arbitrary codimension $1 \leq k-d \leq k-1$. Common examples includes curves and surfaces embedded in $\mathbb{R}^3$, but our results cover the general situation. We develop a general theoretical framework for proving a priori error estimates and bounds on the condition number that relies on abstract properties on the forms involved in the problem. In particular, only certain properties of the stabilization form are required.

We study three different stabilizing forms, one based on the jump in the normal gradient across faces in the active mesh, one based on the full gradient on the active mesh of simplices, and finally, a new stabilizing form based on the surface normal gradient on the active mesh. The consistency error in the normal gradient stabilization is much smaller compared to the full gradient stabilization and therefore more flexible scalings of the stabilization term are possible. Additionally, the normal gradient stabilization works for higher order approximations, and we indicate how to extend the general theoretical framework to cover this situation as well.

We verify that the assumptions on the stabilizing forms in the abstract framework are satisfied for all three stabilizing forms. In the case of surfaces embedded in $\mathbb{R}^3$, the face and full gradient stabilization terms were individually studied in the aforementioned references [4] and [7].

The geometric estimates required to bound the consistency error in the abstract setting are established for the full range of possible codimensions. We start from a very general setting where the discrete manifold is described by a —possibly irregular— triangulation, which is not required to match the background mesh, and which satisfies certain approximation assumptions. Then we establish all the necessary geometry approximation estimates by deriving a semi-explicit, tube-coordinates based representation of the closest point projection and its derivative, which is valid irrespective of the codimension.

We prove interpolation error estimates in this general setting, which extends previous results to higher codimensions. In the case of higher codimensions special care is necessary in the derivation of the interpolation estimate. We note that the standard case of a codimension one hypersurface in $\mathbb{R}^k$ described as a levelset of a piecewise linear continuous function is contained as a special case of our analysis.

While we develop a cut finite element framework for the treatment of the Laplace-Beltrami operator on manifolds with arbitrary codimensions, we only consider piecewise linear approximation spaces. In Grande et al. [18], a similar abstract cut finite element framework is proposed focusing on the higher order treatment of the Laplace-Beltrami operator, but in contrast to our work, the codimension of the considered manifolds is restricted to one.

1.2. **Outline.** The outline of the paper is as follows: We start with recalling the weak formulation of the continuous Laplace-Beltrami problem in Section 2. Then we formulate the abstract stabilized cut finite element framework in Section 3. At the end of Section 3 we discuss a number of concrete realizations including three different choices of the stabilization form. The abstract estimates for the condition number and the a priori error are presented in Section 4 and Section 5, respectively, leading us to a few key assumptions on the stabilization forms. To prepare the verification of these key assumptions, geometric estimates involving the gradient of lifted and extended functions and the change of the domain of integration are established in Section 6. In the same Section we also introduce the concept of "fat intersections" between the discrete manifold and the underlying background mesh. The subsequent Section 7 is devoted to verify the abstract assumptions for the realizations of the stabilization forms. A suitable interpolation operator is presented in Section 8, together with a proof of the interpolation error estimates. The theoretical development is concluded by the verification of the quadrature and consistency properties of the bilinear forms given in Section 9. Finally, in Section 10, we present illustrating numerical examples for surfaces and curves embedded in $\mathbb{R}^3$ that corroborate our theoretical findings.

2. Weak Formulation of the Continuous Model Problem

2.1. **The Continuous Manifold.** In what follows, Γ denotes a smooth compact manifold of dimension d without boundary which is embedded in $\mathbb{R}^k$ and thus has codimension $c = k - d$. For each $y \in \Gamma$, we denote by $N_y\Gamma$ the orthogonal complement of the tangent space $T_y\Gamma$ in $\mathbb{R}^k$,

$$N_y\Gamma = (T_y\Gamma)^\perp = \{v \in \mathbb{R}^k : \langle v, w\rangle = 0 \,\forall\, w \in T_y\Gamma\}. \tag{2.1}$$

Then the normal bundle $N\Gamma$ of Γ is defined as the collection of all normal spaces $N_y\Gamma$; that is

$$N\Gamma = \{(y, v) \in \Gamma \times \mathbb{R}^k : v \in N_y\Gamma\}. \tag{2.2}$$

Locally, the manifold Γ can be equipped with a smooth adapted moving[1] orthonormal frame $\Gamma \ni y \mapsto \{e_i(y)\}_{i=1}^k = \{t_i(y)\}_{i=1}^d \cup \{n_i(y)\}_{i=1}^c$ where $\{t_i(y)\}_{i=1}^d$ and $\{n_i(y)\}_{i=1}^c$ is a orthonormal basis of $T_y\Gamma$ and $N_y\Gamma$, respectively. With the help of such an adapted orthonormal frame, the orthogonal projection P_Γ and Q_Γ of $\mathbb{R}^k$ onto the, respectively, tangent and normal spaces of Γ at $y \in \Gamma$ are given by

$$P_\Gamma = \sum_{i=1}^d t_i \otimes t_i, \qquad Q_\Gamma = \sum_{i=1}^c n_i \otimes n_i, \tag{2.3}$$

or equivalently, since $\mathbb{R}^k = T_y\Gamma \oplus N_y\Gamma \,\forall\, y \in \Gamma$, by

$$Q_\Gamma = I - \sum_{i=1}^d t_i \otimes t_i, \qquad P_\Gamma = I - \sum_{i=1}^c n_i \otimes n_i, \tag{2.4}$$

where I is the identity matrix.

The normal bundle $N\Gamma$ can be used to define adapted coordinates in the δ tubular neighborhood $U_\delta(\Gamma) = \{x \in \mathbb{R}^k : \rho(x) < \delta\}$ where $\rho(x) = \operatorname{dist}(x, \Gamma)$ is the distance function associated to Γ. Introducing the set

$$N_\delta\Gamma = \{(y, v) \in N\Gamma : \|v\|_{\mathbb{R}^k} < \delta\}, \tag{2.5}$$

it is well-known that for a smooth, compact embedded manifold without boundary, the mapping

$$\Psi : N_\delta\Gamma \ni (y, v) \mapsto y + v \in U_\delta(\Gamma) \tag{2.6}$$

in fact defines a diffeomorphism if $0 < \delta \leqslant \delta_0$ for some δ_0 small enough, see, e.g., [1, p.93] for a proof. Assuming from now on that $\delta \leqslant \delta_0$, the closest point projection which maps $x \in U_\delta(\Gamma)$ to its uniquely defined closest point on Γ is given by the smooth retraction

$$p : U_\delta(\Gamma) \ni x \mapsto \Pi \circ \Psi^{-1}(x) \in \Gamma, \tag{2.7}$$

where $\Pi : N\Gamma \ni (q, v) \mapsto q$ is the canonical projection of the normal bundle $N\Gamma$ to its base manifold Γ. The closest point projection allows to extend any function on Γ to its tubular neighborhood $U_\delta(\Gamma)$ using the pull back

$$u^e(x) = u \circ p(x). \tag{2.8}$$

On the other hand, for any subset $\widetilde{\Gamma} \subseteq U_\delta(\Gamma)$ such that $p : \widetilde{\Gamma} \to \Gamma$ defines a bijective mapping, a function w on $\widetilde{\Gamma}$ can be lifted to Γ by the push forward defined by

$$(w^l)(p(x)) = w(x). \tag{2.9}$$

Finally, for any function space V defined on Γ, the space consisting of extended functions is denoted by V^e and correspondingly, the notation V^l refers to the lift of a function space V defined on $\widetilde{\Gamma}$.

[1]The adjective "moving" refers to the fact that the orthonormal basis typically varies (smoothly) over the manifold.

2.2. **The Continuous Weak Problem.** A function $u : \Gamma \to \mathbb{R}$ is of class $C^l(\Gamma)$ if there exists an extension $\overline{u} \in C^l(U)$ with $\overline{u}|_\Gamma = u$ for some k-dimensional neighborhood U of Γ. Using the tangential projection P_Γ, the tangent gradient operator ∇_Γ on Γ can be defined by

$$\nabla_\Gamma u = P_\Gamma \nabla \overline{u}, \tag{2.10}$$

with ∇ being the full $\mathbb{R}^k$ gradient. It can easily be shown that definition (2.10) is independent of the extension $\overline{u}$, see [15, Lemma 2.4]. Then the Laplace-Beltrami operator Δ_Γ on Γ is defined as

$$\Delta_\Gamma = \nabla_\Gamma \cdot \nabla_\Gamma \tag{2.11}$$

and the corresponding weak formulation of problem (1.1) is to seek $u \in H^1(\Gamma)/\mathbb{R}$ such that

$$a(u, v) = l(v) \quad \forall v \in H^1(\Gamma)/\mathbb{R}, \tag{2.12}$$

where

$$a(u, v) = (\nabla_\Gamma u, \nabla_\Gamma v)_\Gamma, \qquad l(v) = (f, v)_\Gamma, \tag{2.13}$$

and $(v, w)_\Gamma = \int_\Gamma vw$ is the L^2 inner product. We let $\|w\|_\Gamma^2 = (w, w)_\Gamma$ denote the $L^2(\Gamma)$ norm on Γ and introduce the Sobolev $H^m(\Gamma)$ space as the subset of L^2 functions for which the norm

$$\|w\|_{m,\Gamma}^2 = \sum_{l=0}^{m} \|D_\Gamma^l w\|_\Gamma^2, \quad m = 0, 1, 2 \tag{2.14}$$

is defined. Here, the L^2 norm for a matrix is based on the pointwise Frobenius norm, $D_\Gamma^0 w = w$ and the derivatives $D_\Gamma^1 w = P_\Gamma \nabla w$, $D_\Gamma^2 w = P_\Gamma(\nabla \otimes \nabla w)P_\Gamma$ are taken in a weak sense. It follows from the Lax-Milgram lemma that the problem (2.12) has a unique solution. For smooth surfaces we also have the elliptic regularity estimate

$$\|u\|_{2,\Gamma} \lesssim \|f\|_\Gamma. \tag{2.15}$$

Here and throughout the paper we employ the notation $\lesssim$ to denote less or equal up to a positive constant which is always independent of the mesh size and the particular cut configuration, but may be dependent on the dimensions k and d, the shape regularity of the mesh and the curvature of the manifold. The binary relations $\gtrsim$ and $\sim$ are defined analogously.

3. The Abstract Cut Finite Element Formulation

The cut finite element formulation for the numerical solution of (2.12) is based on two ingredients. First, a geometric approximation Γ_h of the embedded manifold Γ has be to provided which facilitates the numerical computation of the discrete counterpart of (2.12). Second, a discretization of (a neighborhood) of the embedding space $\mathbb{R}^k$ is required to provide the approximation spaces in which the numerical solution will be sought. We start with specifying the requirements for Γ_h.

3.1. **The Discrete Manifold.** For Γ_h, let $\mathcal{K}_h = \{K\}$ be a conform mesh without boundary consisting of d dimensional simplices K. While we do not require that the simplices are shape-regular, we assume that they are non-degenerated. On $\Gamma_h = \bigcup_{K \in \mathcal{K}_h} K$ we can then define the piecewise constant, discrete tangential projection P_{Γ_h} as the orthogonal projection on the d-dimensional (affine) subspace defined by each $K \in \mathcal{K}_h$. We assume that:

- $\Gamma_h \subset U_{\delta_0}(\Gamma)$ and that the closest point mapping $p : \Gamma_h \to \Gamma$ is a bijection for $0 < h \leq h_0$.
- The following estimates hold

$$\|\rho\|_{L^\infty(\Gamma_h)} \lesssim h^2, \qquad \|P_\Gamma^e - P_{\Gamma_h}\|_{L^\infty(\Gamma_h)} \lesssim h. \tag{3.1}$$

Before we proceed, we observe that the assumption on the convergence of the tangential projectors can be reformulated as follows:

Lemma 3.1. *The following assumptions are equivalent.*

(1) There exists a piecewise smooth moving orthonormal tangential frame $\{t_i^h\}_{i=1}^d$ such that

$$\|t_i^e - t_i^h\|_{L^\infty(\Gamma_h)} \lesssim h \quad \text{for } i = 1, \dots, d. \tag{3.2}$$

(2) The discrete tangential projection P_{Γ_h} satisfies

$$\|P_\Gamma^e - P_{\Gamma_h}\|_{L^\infty(\Gamma_h)} \lesssim h. \tag{3.3}$$

(3) There exists a piecewise smooth moving orthonormal normal frame $\{n_i^h\}_{i=1}^c$ such that

$$\|n_i^e - n_i^h\|_{L^\infty(\Gamma_h)} \lesssim h \quad \text{for } i = 1, \dots, c. \tag{3.4}$$

(4) The discrete normal projection Q_{Γ_h} satisfies

$$\|Q_\Gamma^e - Q_{\Gamma_h}\|_{L^\infty(\Gamma_h)} \lesssim h. \tag{3.5}$$

Proof. The proof is elementary and included only for completeness. Clearly, with

$$P_{\Gamma_h} = \sum_{i=1}^{d} t_i^h \otimes t_i^h, \qquad Q_{\Gamma_h} = \sum_{i=1}^{c} n_i^h \otimes n_i^h, \tag{3.6}$$

(1) $\Rightarrow$ (2) and (3) $\Rightarrow$ (4). Moreover, since $I = P_{\Gamma_h} + Q_{\Gamma_h}$, the assumptions (2) and (4) are clearly equivalent. It remains to show that existence of either the discrete normal or tangential projector with the assumed convergence properties implies the existence of a corresponding discrete normal and tangential frame. For $K \in \mathcal{K}_h$, we take a smooth orthonormal frame $\{E_i\}_{i=1}^k = \{t_i\}_{i=1}^d \cup \{n_i\}_{i=1}^c$ on $K^l = p(K)$. Set $\widetilde{t}_i^h = P_{\Gamma_h}(t_i^e)$ and $\widetilde{n}_i^h = Q_{\Gamma_h}(n_i^e)$ and observe that $\|t_i^e - \widetilde{t}_i^h\|_{L^\infty(\Gamma_h)} = \|(P_\Gamma^e - P_{\Gamma_h})(t_i^e)\|_{L^\infty(\Gamma_h)} \lesssim h$ and similar for $\widetilde{n}_i^h$. Consequently, the frame $\{\widetilde{E}_i^h\}$ which consists of discrete tangent vectors $\{\widetilde{t}_i^h\}_{i=1}^d$ and discrete normal vectors $\{\widetilde{n}_i\}_{i=1}^c$ defines an almost orthonormal basis of $\mathbb{R}^k$ for h small enough since $\langle \widetilde{E}_i^h, \widetilde{E}_j^h \rangle = \delta_{ij} + h$ by the approximation properties of the projectors. Applying a Gram-Schmidt orthonormalization procedure to both frames $\{\widetilde{t}_i^h\}_{i=1}^d$ and $\{\widetilde{n}_i^h\}_{i=1}^c$ separately, constructs a discrete orthonormal frame $\{t_i^h\}_{i=1}^d \cup \{n_i^h\}_{i=1}^c$ on K. As the orthonormalization procedure involves only C^∞ operations, $\|\widetilde{t}_i^h - t_i^h\|_{L^\infty(K)} \lesssim h$ and $\|\widetilde{n}_i^h - n_i^h\|_{L^\infty(K)} \lesssim h$ and thus the constructed discrete orthonormal normal and tangential frames satisfy the desired approximation property. □

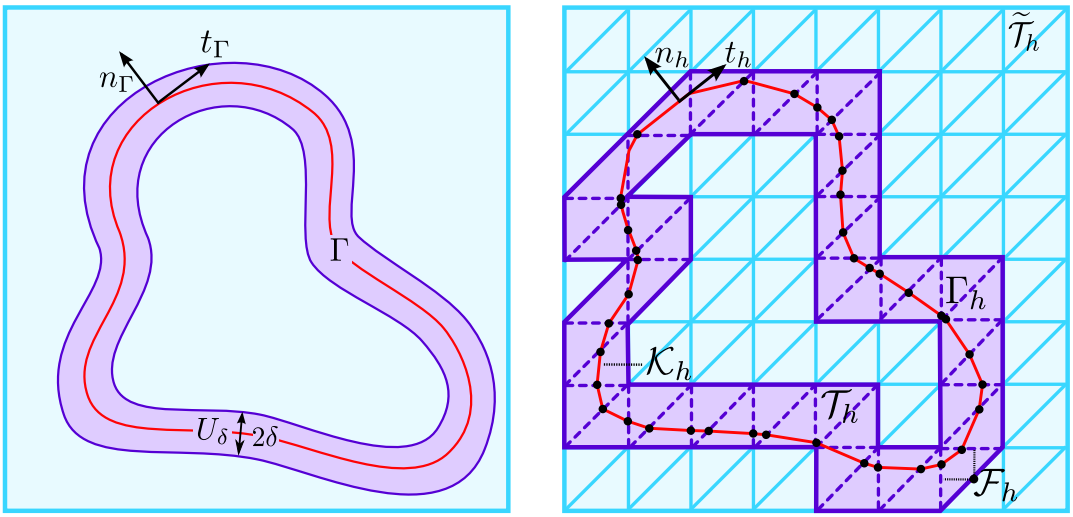

FIGURE 1. Set-up of the continuous and discrete domains. (Left) Continuous surface Γ enclosed by a δ tubular neighborhood $U_\delta(\Gamma)$. (Right) Discrete manifold Γ_h embedded into a background mesh $\widetilde{\mathcal{T}}_h$ from which the active (background) mesh $\mathcal{T}_h$ is extracted.

3.2. **Stabilized Cut Finite Element Methods.** Let $\widetilde{\mathcal{T}}_h$ be a quasi-uniform mesh, with mesh parameter $0 < h \leq h_0$ and consisting of shape regular closed simplices, of some open and bounded domain $\Omega \subset \mathbb{R}^k$ containing the embedding neighborhood $U_{\delta_0}(\Gamma)$. For the background mesh $\widetilde{\mathcal{T}}_h$ we define the *active* (background) mesh $\mathcal{T}_h$ and its set of *interior* faces $\mathcal{F}_h$ by

$$\mathcal{T}_h = \{T \in \widetilde{\mathcal{T}}_h : T \cap \Gamma_h \neq \emptyset\}, \tag{3.7}$$

$$\mathcal{F}_h = \{F = T^+ \cap T^- : T^+, T^- \in \mathcal{T}_h\}, \tag{3.8}$$

and for the domain covered by $\mathcal{T}_h$ we introduce the notation

$$N_h = \cup_{T \in \mathcal{T}_h} T. \tag{3.9}$$

Note that for any element $T \in \mathcal{T}_h$ there is a neighbor $T' \in \mathcal{T}_h$ such that T and T' share a face. We assume that the partition $\mathcal{K}_h$ of Γ_h is compatible with the active mesh in the sense that

$$\forall\, K \in \mathcal{K}_h : K \cap T \neq \emptyset \Rightarrow K \subset T. \tag{3.10}$$

Such a compatible partition $\mathcal{K}_h$ can always be generated starting from an initial partition $\widetilde{\mathcal{K}}_h$ by subtriangulating non-empty intersections $K \cap T$. The various set of geometric entities are illustrated in Figure 1.

On the active mesh $\mathcal{T}_h$ we introduce the discrete space of continuous piecewise linear polynomials

$$V_h = \{v \in C(N_h) : v|_T \in P_1(T)\ \forall\, T \in \mathcal{T}_h\}, \tag{3.11}$$

and its normalized members having zero average constitute the normalized discrete function space

$$V_{h,0} = \{v \in V_h : \lambda_{\Gamma_h}(v) = 0\}, \tag{3.12}$$

where $\lambda_{\Gamma_h}(v) = \frac{1}{|\Gamma_h|}\int_{\Gamma_h} v$ is the average of v on Γ_h. Then the general form of the stabilized cut finite element method for the Laplace-Beltrami problem (1.1) is to seek $u_h \in V_{h,0}$ such that

$$a_h(u_h, v) + s_h(u_h, v) = l_h(v) \quad \forall v \in V_{h,0}. \tag{3.13}$$

Here, a_h and l_h denote discrete counterparts of the continuous bilinear a and linear form l, respectively, and are defined on Γ_h, while s_h represents a stabilization term, see (3.22) and Table 1 for concrete realizations of these forms. Both a_h and s_h are supposed to be symmetric and positive semidefinite. The role of the stabilization is to enhance the stability properties of the discrete bilinear form a_h in such a way that geometrically robust optimal condition number and a priori error estimates can be derived which are independent of the position of Γ_h relative to $\mathcal{T}_h$. Additionally, to facilitate the abstract analysis of the condition number and a priori error bounds for formulation (3.13), the discrete forms need to satisfy certain assumptions which will be defined in Section 4 and 5. Specific realizations will be discussed in Section 3.3.

In the course of the forthcoming abstract numerical analysis, we will make use of the stabilization (semi)-norm

$$\|v\|_{s_h}^2 = s_h(v, v), \tag{3.14}$$

as well as of the following energy norms defined for $v \in H^1(\Gamma) + (V_h|_{\Gamma_h})^l$ and $w \in H^1(\Gamma)^e + V_h|_{\Gamma_h}$

$$\|v\|_a^2 = a(v, v), \quad \|w\|_{a_h}^2 = a_h(w, w), \quad \|w\|_{A_h}^2 = A_h(w, w) = \|w\|_{a_h}^2 + \|w\|_{s_h}^2, \tag{3.15}$$

where A_h denotes the overall symmetric, discrete bilinear form

$$A_h(v, w) = a_h(v, w) + s_h(v, w) \quad \forall\, v, w \in V_{h,0}. \tag{3.16}$$

Additionally, we assume that $\|\cdot\|_{A_h}$ defines a stronger norm than $\|\cdot\|_a$ in the sense that

$$\|v\|_a \lesssim \|v^e\|_{A_h}, \qquad \|w^l\|_a \lesssim \|w\|_{A_h}. \tag{3.17}$$

Clearly, the abstract bilinear form (3.16) is both coercive and continuous with respect to $\|\cdot\|_{A_h}$

$$\|v\|_{A_h}^2 \lesssim A_h(v, v), \tag{3.18}$$

$$A_h(v, w) \lesssim \|v\|_{A_h}\|w\|_{A_h}. \tag{3.19}$$

Remark 3.2 (Higher order methods). To obtain higher order discretization schemes, the cut finite element space 3.11 and the geometric assumptions (3.1) have to be replaced by their respective high order counterparts. More precisely, using the continuous piecewise polynomial space of order l,

$$V_h^l = \{v \in C(N_h) : v|_T \in P_l(T) \; \forall T \in \mathcal{T}_h\}, \tag{3.20}$$

the geometric approximation error needs to satisfy

$$\|\rho\|_{L^\infty(\Gamma_h)} \lesssim h^{l+1}, \qquad \|P_\Gamma^e - P_{\Gamma_h}\|_{L^\infty(\Gamma_h)} \lesssim h^l. \tag{3.21}$$

Additionally, the stabilization term s_h needs to obey an appropriate weak consistency assumption, see Remark 5.3.

3.3. **Realizations of the Abstract Cut Finite Element Method.** We conclude the introduction of the abstract cut finite element method (3.13) by defining and briefly discussing a number of concrete realizations of the discrete bilinear form a_h and the stabilization form s_h as summarized in Table 1. Here and throughout the remaining work, the following notation is used. Any norm $\|\cdot\|_{\mathcal{P}^h}$ which involves a collection of geometric entities $\mathcal{P}^h$ should be understood as broken norm defined by $\|\cdot\|_{\mathcal{P}^h}^2 = \sum_{P\in\mathcal{P}^h} \|\cdot\|_P^2$ whenever $\|\cdot\|_P$ is well-defined, with a similar convention for scalar products $(\cdot,\cdot)_{\mathcal{P}^h}$. Furthermore, any set operations involving $\mathcal{P}^h$ are also understood as element-wise operations, e.g., $\mathcal{P}^h \cap U = \{P \cap U \mid P \in \mathcal{P}^h\}$. With this notation, the discrete linear form l_h considered in this work can be expressed by

$$l_h(v) = (f^e, v)_{\mathcal{K}_h}. \tag{3.22}$$

For the discrete bilinear form a_h we consider two variants, one built upon the discrete tangential gradient while the second variant replaces the discrete tangential gradient with the full gradient, similar to the surface PDE methods considered in [10, 31]. Next, we recall that stabilization

Discrete bilinear forms	$a_h(u,v)$
Tangential gradient	$a_h^1(v,w) = (\nabla_{\Gamma_h} v, \nabla_{\Gamma_h} w)_{\Gamma_h}$
Full gradient	$a_h^2(v,w) = (\nabla v, \nabla w)_{\Gamma_h}$
Stabilization forms	$s_h(u,v)$
Face-based	$s_h^1(v,w) = \tau h^{1-c}(n_F \cdot [\nabla v], n_F \cdot [\nabla w])_{\mathcal{F}_h}$
Full gradient	$s_h^2(v,w) = \tau h^{2-c}(\nabla v, \nabla w)_{\mathcal{T}_h}$
Normal gradient	$s_h^3(v,w) = \tau h^{\alpha-c}(Q_{\Gamma_h}^e \nabla v, Q_{\Gamma_h}^e \nabla w)_{\mathcal{T}_h}, \qquad \alpha \in [0,2]$

TABLE 1. Realizations of the discrete bilinear form a_h and stabilization form s_h, the latter is weighted with a dimensionless stabilization parameter $\tau > 0$.

operators s_h using a face-based gradient jump penalization and an artificial diffusion like, full gradient stabilization were introduced in [4] and [7] for various cut finite element discretizations of the Laplace-Beltrami problem on surfaces. Here, we generalized these stabilization operators to work with cut finite element formulations on manifolds of arbitrary codimension. Additionally, motivated by the fact that the normal gradient $Q_\Gamma \nabla v^e$ for any normal extension of a function $v \in H^1(\Gamma)$ vanishes, we propose a novel stabilization which penalizes the discrete normal gradient, see Table 1.

Remark 3.3. Compared to the face-based stabilization s_h^1, the full gradient stabilization s_h^2, has three main advantages: First, its implementation is extremely cheap and immediately available in many finite element codes. Second, the stencil of the discretization operator is not enlarged, as opposed to using a face-based penalty operator. Third, numerical studies for the surface case

indicate that the accuracy and conditioning of a full gradient stabilized surface method is less sensitive to the choice of the stability parameter τ than for a face-based stabilized scheme, see [7].

Remark 3.4. While the full gradient stabilization has a number of advantages, its use is limited to low-order P_1 methods due to its inconsistency. The inconsistency of the normal gradient stabilization on the other hand is purely caused by geometric approximation errors of the normal field encoded in the mapping $Q_{\Gamma_h} \circ P_\Gamma$, see the proof of Lemma (6.4). This has two consequences. First, it gives us more freedom for the choice of the h-scaling in s_h^3 and the possibility to tune the control of the normal gradient component of the computed discrete solution. Second, the stabilization is weakly consistent also for high-order P_k methods $k \geqslant 1$ when the appropriate geometric approximation properties $\|\rho\|_{L^\infty(\Gamma_h)} \lesssim h^{k+1}$ and $\|Q_\Gamma^e - Q_{\Gamma_h}\|_{L^\infty(\Gamma_h)} \lesssim h^k$ are met.

Remark 3.5. While the implementation of the face-based stabilization s_h^1 and the full gradient stabilization s_h^2 is rather straight-forward and independent of the codimension and construction of Γ_h as they do not rely on any geometrical information on Γ_h, the realization of the normal gradient stabilization can be more delicate. For codimension-1 manifold implicitly defined by a level set $\{\phi = 0\}$, the discrete normal field can be constructed by defining $n_h = \frac{\nabla \pi_h \phi}{|\nabla \pi_h \phi|}$, where π_h is suitable interpolation operator associated with V_h. Similarly, if the manifold Γ of codimension c is defined as the intersection of c non-transversal level sets $\{\phi_i = 0\}$, $i = 1, \dots, c$, a discrete normal bundle can be computed in given set of quadrature points by orthonormalization the normal space basis consisting of $\{n_h^i\}_{i=1}^c = \{\nabla \pi_h \phi / |\nabla \pi_h \phi|\}_{i=1}^c$, provided that the discrete level sets $\{\pi_h \phi_i = 0\}$, $i = 1, \dots, c$ are transversal in the quadrature points.

Remark 3.6. Very recently, a new stabilization term was proposed in [25] which similar to the normal gradient volume stabilization s_h^3 works for higher order elements. It combines properly scaled, higher order normal derivatives on the surface with the corresponding higher order variant of s_h^1 introduced in [2].

4. Abstract Condition Number Estimates

In this section, we formulate two abstract assumptions on the stabilized bilinear form (3.16) which allow us to establish optimal condition number bounds for the associated discrete system which are independent of the position of the manifold Γ_h relative to the background mesh $\mathcal{T}_h$. Following the approach in [16], we require that for $v \in V_{h,0}$, the discrete bilinear form A_h satisfies

- **a discrete Poincaré estimate**

$$h^{-c} \|v - \lambda_{\Gamma_h}(v)\|_{\mathcal{T}_h}^2 \lesssim \|v\|_{A_h}^2, \tag{4.1}$$

- **an inverse estimate** of the form

$$\|v\|_{A_h}^2 \lesssim h^{-2-c} \|v\|_{\mathcal{T}_h}^2, \tag{4.2}$$

with the hidden constants being independent of the manifold position in the background mesh.

Remark 4.1. Note that an immediate consequence of (4.1) is that $\|\cdot\|_{A_h}$ indeed defines a norm on the normalized discrete space $V_{h,0}$.

Next, we define the stiffness matrix $\mathcal{A}$ associated with the bilinear form A_h by the relation

$$(\mathcal{A}V, W)_{\mathbb{R}^N} = A_h(v, w) \quad \forall\, v, w \in V_h, \tag{4.3}$$

where $V = \{V_i\}_{i=1}^N \in \mathbb{R}^N$ is the expansion coefficient vector for $v_h \in V_h$ with respect to the standard piecewise linear basis functions $\{\phi_i\}_{i=1}^N$ associated with $\mathcal{T}_h$; that is, $v = \sum_{i=1}^N V_i \phi_i$. Recall that for a quasi-uniform mesh $\mathcal{T}_h$, the coefficient vector V satisfies the well-known estimate

$$h^{k/2} \|V\|_{\mathbb{R}^N} \lesssim \|v_h\|_{L^2(\mathcal{T}_h)} \lesssim h^{k/2} \|V\|_{\mathbb{R}^N}. \tag{4.4}$$

The fulfillment of the discrete Poincaré estimate (4.1) ensures that the stiffness matrix $\mathcal{A}$ is a bijective linear mapping $\mathcal{A} : \widehat{\mathbb{R}}^N \to \ker(\mathcal{A})^\perp$ where we set $\widehat{\mathbb{R}}^N = \mathbb{R}^N / \ker(\mathcal{A})$ to factor out the

one-dimensional kernel given by $\ker \mathcal{A} = \operatorname{span}\{(1,\dots,1)^T\}$. For the matrix $\mathcal{A}$, its operator norm and condition number are defined by

$$\|\mathcal{A}\|_{\mathbb{R}^N} = \sup_{V\in\widehat{\mathbb{R}}^N\setminus\mathbf{0}} \frac{\|\mathcal{A}V\|_{\mathbb{R}^N}}{\|V\|_{\mathbb{R}^N}} \quad \text{and} \quad \kappa(\mathcal{A}) = \|\mathcal{A}\|_{\mathbb{R}^N}\|\mathcal{A}^{-1}\|_{\mathbb{R}^N}, \tag{4.5}$$

respectively. Then combining the mass matrix scaling (4.4) with the Poincaré estimate (4.1), the inverse estimate (4.2) and the boundedness (3.19) of A_h, the abstract approach in [16] allows to establish the following bound for the condition number:

Theorem 4.2. *The condition number of the stiffness matrix satisfies the estimate*

$$\kappa(\mathcal{A}) \lesssim h^{-2}, \tag{4.6}$$

where the hidden constant depends only on the quasi-uniformity parameter.

Proof. We need to bound $\|\mathcal{A}\|_{\mathbb{R}^N}$ and $\|\mathcal{A}^{-1}\|_{\mathbb{R}^N}$. First observe that for $w \in V_h$,

$$\|w\|_{A_h} \lesssim h^{-(2+c)/2}\|w\|_{\mathcal{T}_h} \lesssim h^{(k-2-c)/2}\|W\|_{\mathbb{R}^N} = h^{(d-2)/2}\|W\|_{\mathbb{R}^N}, \tag{4.7}$$

where the inverse estimate (4.2) and equivalence (4.4) were successively used. Consequently,

$$\|\mathcal{A}V\|_{\mathbb{R}^N} = \sup_{W\in\mathbb{R}^N} \frac{(\mathcal{A}V,W)_{\mathbb{R}^N}}{\|W\|_{\mathbb{R}^N}} = \sup_{w\in V_h} \frac{A_h(v,w)}{\|w\|_{A_h}} \frac{\|w\|_{A_h}}{\|W\|_{\mathbb{R}^N}} \lesssim h^{(d-2)/2}\|v\|_{A_h} \lesssim h^{d-2}\|V\|_{\mathbb{R}^N}, \tag{4.8}$$

and thus $\|\mathcal{A}\|_{\mathbb{R}^N} \lesssim h^{d-2}$ by the definition of the operator norm. To estimate $\|\mathcal{A}^{-1}\|_{\mathbb{R}^N}$, start from (4.4) and combine the Poincaré inequality (4.1) with a Cauchy-Schwarz inequality to arrive at the following chain of estimates:

$$\|V\|^2_{\mathbb{R}^N} \lesssim h^{-k}\|v\|^2_{\mathcal{T}_h} \lesssim h^{c-k}A_h(v,v) = h^{-d}(V,\mathcal{A}V)_{\mathbb{R}^N} \lesssim h^{-d}\|V\|_{\mathbb{R}^N}\|\mathcal{A}V\|_{\mathbb{R}^N}, \tag{4.9}$$

and hence $\|V\|_{\mathbb{R}^N} \lesssim h^{-d}\|\mathcal{A}V\|_{\mathbb{R}^N}$. Now setting $V = \mathcal{A}^{-1}W$ we conclude that $\|\mathcal{A}^{-1}\|_{\mathbb{R}^N} \lesssim h^{-d}$ and combining estimates for $\|\mathcal{A}\|_{\mathbb{R}^N}$ and $\|\mathcal{A}^{-1}\|_{\mathbb{R}^N}$ the theorem follows. □

5. Abstract A Priori Error Analysis

This section is devoted to the abstract analysis of the a priori error for the weak formulation (3.13). First, we derive two abstract Strang-type lemmas which show that the total energy and L^2 error can be split into interpolation, quadrature and consistency errors. Then we present general assumptions that the discrete forms a_h, s_h and l_h must satisfy in order to ensure that the resulting cut finite element method (3.13) defines a optimally convergent discretization scheme.

5.1. Two Strang-type Lemmas.

We start with a Strang-type lemma for the energy error.

Lemma 5.1. *Let u be the solution of (1.1) and u_h the solution of (3.13). Then*

$$\|u^e - u_h\|_{A_h} \lesssim \inf_{v_h\in V_h} \|u^e - v_h\|_{A_h} + \sup_{v_h\in V_h\setminus\{0\}} \frac{l_h(v_h) - A_h(u^e,v_h)}{\|v_h\|_{A_h}} \tag{5.1}$$

$$\lesssim \inf_{v_h\in V_h} \|u^e - v_h\|_{A_h} + \sup_{v_h\in V_h\setminus\{0\}} \frac{l_h(v_h) - l(v_h^l)}{\|v_h\|_{A_h}} + \sup_{v_h\in V_h\setminus\{0\}} \frac{a(u,v_h^l) - a_h(u^e,v_h)}{\|v_h\|_{A_h}}$$
$$+ \sup_{v\in V_h\setminus\{0\}} \frac{s_h(u^e,v_h)}{\|v_h\|_{A_h}}. \tag{5.2}$$

Proof. Thanks to the triangle inequality $\|u^e - u_h\|_{A_h} \leqslant \|u^e - v_h\|_{A_h} + \|u_h - v_h\|_{A_h}$ with $v \in V_h$, it is enough to proceed with the "discrete error" $e_h = u_h - v_h$. Observe that

$$\|e_h\|^2_{A_h} = A_h(u_h - v_h, e_h) \tag{5.3}$$

$$= l_h(e_h) - A_h(u^e,e_h) + A_h(u^e - v_h, e_h) \tag{5.4}$$

$$\lesssim \left(\sup_{v\in V_h\setminus\{0\}} \frac{l_h(v_h) - A_h(u^e,v_h)}{\|v_h\|_{A_h}} + \sup_{v_h\in V_h\setminus\{0\}} \frac{A_h(u^e - v_h, v_h)}{\|v_h\|_{A_h}} \right) \|e_h\|_{A_h}. \tag{5.5}$$

Dividing by $\|e_h\|_{A_h}$ and applying a Cauchy-Schwarz inequality to the second remaining term in (5.5) gives (5.1). To prove the second estimate (5.2), simply observe that the identity

$$l_h(v_h) - A_h(u^e, v_h) = \big(l_h(v_h) - l(v_h^l)\big) + \big(a(u, v_h^l) - a_h(u^e, v_h)\big) - s_h(u^e, v_h). \tag{5.6}$$

follows directly from inserting $l(v_h^l) - a(u, v_h^l) = 0$ into (5.5). □

Next, we derive a corresponding representation for the L^2 error using the standard Aubin-Nitsche duality argument.

Lemma 5.2. *With u the solution of (1.1) and u_h the solution of (3.13) it holds for any $\phi_h \in V_h$*

$$\|u - u_h^l\|_\Gamma \lesssim \|u - u_h^l\|_a \sup_{\phi \in H^2(\Gamma)\setminus\{0\}} \frac{\|\phi - \phi_h^l\|_a}{\|\phi\|_{2,\Gamma}} + \sup_{\phi \in H^2(\Gamma)} \frac{l(\phi_h) - a(u_h^l, \phi_h^l)}{\|\phi\|_{2,\Gamma}} + \|\lambda_\Gamma(u_h^l)\|_\Gamma \tag{5.7}$$

$$\lesssim \|u - u_h^l\|_a \sup_{\phi \in H^2(\Gamma)\setminus\{0\}} \frac{\|\phi - \phi_h^l\|_a}{\|\phi\|_{2,\Gamma}} + \sup_{\phi \in H^2(\Gamma)\setminus\{0\}} \frac{l(\phi_h^l) - l_h(\phi_h)}{\|\phi\|_{2,\Gamma}}$$

$$+ \sup_{\phi \in H^2(\Gamma)\setminus\{0\}} \frac{a_h(u_h, \phi_h) - a(u_h^l, \phi_h^l)}{\|\phi\|_{2,\Gamma}} + \sup_{\phi \in H^2(\Gamma)\setminus\{0\}} \frac{s_h(u_h, \phi_h)}{\|\phi\|_{2,\Gamma}} + \|\lambda_\Gamma(u_h^l)\|_\Gamma. \tag{5.8}$$

Proof. First, we decompose the error $e = u - u_h^l$ into a normalized part $\tilde{e}$ satisfying $\lambda_\Gamma(\tilde{e}) = 0$ and a constant part,

$$e = u - u_h^l = \underbrace{u - (u_h^l - \lambda_\Gamma(u_h^l))}_{\tilde{e}} - \lambda_\Gamma(u_h^l). \tag{5.9}$$

By the triangle inequality $\|e\|_\Gamma \leqslant \|\tilde{e}\|_\Gamma + \|\lambda_\Gamma(u_h^l)\|_\Gamma$, it suffices to proceed with $\|\tilde{e}\|_\Gamma$. Now let $\psi \in L_0^2(\Gamma)$ and take $\phi \in H^2(\Gamma)$ satisfying $-\Delta_\Gamma \phi = \psi$ and the elliptic regularity estimate $\|\phi\|_{2,\Gamma} \lesssim \|\psi\|_\Gamma$, see (2.15). Then the normalized error $\tilde{e}$ can be represented as $(\tilde{e}, \psi)_\Gamma = a(\tilde{e}, \phi) = a(e, \phi)$ and adding and subtracting any lifted finite element function ϕ_h^l gives

$$\|\tilde{e}\|_\Gamma = \sup_{\psi \in L_0^2(\Gamma)\setminus\{0\}} \frac{(\tilde{e}, \psi)_\Gamma}{\|\psi\|_\Gamma} \tag{5.10}$$

$$\lesssim \sup_{\phi \in H^2(\Gamma)\setminus\{0\}} \frac{a(e, \phi)}{\|\phi\|_{2,\Gamma}} \tag{5.11}$$

$$\lesssim \sup_{\phi \in H^2(\Gamma)\setminus\{0\}} \frac{a(e, \phi - \phi_h^l)}{\|\phi\|_{2,\Gamma}} + \sup_{\phi \in H^2(\Gamma)\setminus\{0\}} \frac{a(e, \phi_h^l)}{\|\phi\|_{2,\Gamma}} \tag{5.12}$$

$$\lesssim \|u - u_h^l\|_a \sup_{\phi \in H^2(\Gamma)\setminus\{0\}} \frac{\|\phi - \phi_h^l\|_a}{\|\phi\|_{2,\Gamma}} + \sup_{\phi \in H^2(\Gamma)\setminus\{0\}} \frac{l(\phi_h^l) - a(u_h^l, \phi_h^l)}{\|\phi\|_{2,\Gamma}}, \tag{5.13}$$

which proves (5.7). Similar as in the proof of the previous Strang Lemma, the second estimate (5.8) follows from inserting $a_h(u_h, \phi_h) + s_h(u_h, \phi_h) - l_h(\phi_h) = 0$ into the second term of (5.13). □

5.2. **A Priori Error Estimates.** Motivated by the abstract Strang-type lemma for the energy and L^2 norm error, we now assume that the following estimates hold in order to derive optimal bounds for the a priori error of the abstract cut finite element formulation (3.13):

- **Interpolation estimates.** There exists an interpolation operator $\pi_h : H^2(\Gamma) \to V_h$ such that for $v \in H^2(\Gamma)$ it holds

$$\|v^e - \pi_h v^e\|_{\Gamma_h} + h\|v^e - \pi_h v^e\|_{A_h} \lesssim h^2 \|v\|_{2,\Gamma}. \tag{5.14}$$

- **Quadrature estimates.** To prove optimal energy error estimates, we assume that for $v \in V_h$ and a finite element approximation $u_h \in V_h$ of $u \in H^2(\Gamma)$, it holds

$$|l_h(v) - l(v^l)| \lesssim h\|f\|_\Gamma \|v\|_{A_h}, \tag{5.15}$$

$$|a(u, v^l) - a_h(u^e, v)| \lesssim h\|u\|_{2,\Gamma} \|v\|_{A_h}. \tag{5.16}$$

Moreover, in order to obtain an optimal bound for the L^2 error using the standard Nitsche-Aubin duality trick, we require that the improved estimates

$$|l_h(\phi_h) - l(\phi_h^l)| \lesssim h^2 \|f\|_\Gamma \|\phi\|_{2,\Gamma}, \tag{5.17}$$

$$|a(u_h^l, \phi_h^l) - a_h(u_h, \phi_h)| \lesssim h^2 \|u\|_{2,\Gamma} \|\phi\|_{2,\Gamma}, \tag{5.18}$$

hold, whenever ϕ_h is a suitable finite element approximation of $\phi \in H^2(\Gamma)$.

- **Consistency error estimate.** Finally, we require that the stabilization term s_h is weakly consistent in the sense that for $\forall\, v \in H^2(\Gamma)$

$$\|v^e\|_{s_h} \lesssim h \|v\|_{2,\Gamma}. \tag{5.19}$$

Remark 5.3. To cover higher order cut finite element schemes using continuous piecewise polynomials of order l, the assumed interpolation, quadrature and consistency error estimates of order $\mathcal{O}(h)$ and $\mathcal{O}(h^2)$ have to be replaced by $\mathcal{O}(h^l)$ and $\mathcal{O}(h^{l+1})$, respectively. In particular, the stabilization form s_h needs to be designed in such a way that it satisfies the weak consistency estimate

$$\|v^e\|_{s_h} \lesssim h^l \|v\|_{l+1,\Gamma} \quad \forall\, v \in H^{l+1}(\Gamma). \tag{5.20}$$

If assumptions on the interpolation, quadrature and consistency errors are met, it is easy to prove the following theorem.

Theorem 5.4. *Let $u \in H^2(\Gamma)$ be the solution to continuous problem (1.1) and u_h be the solution to the discrete problem (3.13). Then the following a priori error estimates hold*

$$\|u^e - u_h\|_{A_h} \lesssim h \|f\|_\Gamma, \tag{5.21}$$

$$\|u - u_h^l\|_\Gamma \lesssim h^2 \|f\|_\Gamma. \tag{5.22}$$

Proof. The proof of the energy estimate (5.21) follows directly from the Strang lemma (5.2) and assumptions (5.14), (5.15)–(5.16) and (5.19), only noting that $s_h(u_h, v) \leqslant \|u_h\|_{s_h} \|v\|_{A_h}$ thanks to the symmetry of s_h and the definition of $\|\cdot\|_{A_h}$.

To prove the L^2 error estimate (5.22), it only remains to have a closer look at the first and two last terms in Strang lemma (5.8). Set $\phi_h = \pi_h \phi$ and observe that by assumption (3.17), $\|u - u_h^l\|_a \lesssim \|u^e - u_h\|_{A_h}$ and $\|\phi - \phi_h^l\|_a \lesssim \|\phi^e - \phi_h\|_{A_h}$. Thus, the first term in (5.8) can be bounded by $\|u - u_h^l\|_a \|\phi - \phi_h^l\|_a \lesssim h^2 \|f\|_\Gamma \|\phi\|_{2,\Gamma}$. Next, the estimates for the energy, interpolation and consistency error give in combination with a Cauchy-Schwarz inequality and the regularity result (2.15) the following bound

$$s_h(u_h, \phi_h) = s_h(u_h - u^e, \phi_h) + s_h(u^e, \phi_h) \tag{5.23}$$

$$= s_h(u_h - u^e, \phi_h - \phi^e) + s_h(u_h - u^e, \phi^e) + s_h(u^e, \phi^e) + s_h(u^e, \phi_h - \phi^e) \tag{5.24}$$

$$\lesssim h \|f\|_\Gamma h \|\phi\|_{2,\Gamma}. \tag{5.25}$$

To estimate the deviation of the lifted function u_h^l from the 0-average encoded in $\|\lambda_\Gamma(u_h^l)\|_\Gamma$, we will use the notation and results established in Section 6.3. Simply insert $\lambda_{\Gamma_h}(u_h) = 0$ and unwind the definition of the average operators $\lambda_{\Gamma_h}(\cdot)$ and $\lambda_\Gamma(\cdot)$ to see that

$$\|\lambda_\Gamma(u_h^l)\|_\Gamma = |\Gamma|^{\frac{1}{2}} \left| \frac{1}{|\Gamma|} \int_\Gamma u_h^l \,\mathrm{d}\Gamma - \frac{1}{|\Gamma_h|} \int_{\Gamma_h} u_h \,\mathrm{d}\Gamma_h \right| \lesssim \frac{|\Gamma|^{\frac{1}{2}}}{|\Gamma_h|} \int_{\Gamma_h} |1 - c||u_h| \,\mathrm{d}\Gamma_h, \tag{5.26}$$

with $c = |\Gamma_h||\Gamma|^{-1}|B|_d$. Here, $|B|_d$ refers to the change of measure between Γ and Γ_h, see (6.42) for the definition. Anticipating the geometric estimates to be established in Section 6.3, we observe that $\|1 - c\|_{L^\infty(\Gamma)} \lesssim h^2$ thanks to (6.43). Consequently, after successively applying a Cauchy-Schwarz inequality, the inverse estimate (7.4), the discrete Poincaré estimate (4.1), and finally, the stability bound $\|u_h\|_{A_h} \lesssim \|f\|_\Gamma$, we arrive at the desired estimate,

$$\|\lambda_\Gamma(u_h^l)\|_\Gamma \lesssim \frac{|\Gamma|^{\frac{1}{2}}}{|\Gamma_h|} h^2 \|u_h\|_{L^1(\Gamma_h)} \lesssim \frac{|\Gamma|^{\frac{1}{2}}}{|\Gamma_h|^{\frac{1}{2}}} h^2 \|u_h\|_{\Gamma_h} \lesssim h^2 h^{-\frac{c}{2}} \|u_h\|_{\mathcal{T}_h} \lesssim h^2 \|u_h\|_{A_h} \lesssim h^2 \|f\|_\Gamma. \tag{5.27}$$

□

6. Geometric Estimates and Properties

The aim of this section is to develop and collect those geometric properties, identities and estimates which will be needed in the forthcoming verification of the abstract key assumptions (4.1)–(4.2), (5.15)–(5.18) and (5.19), as well as in construction of a suitable interpolation operator satisfying (5.14). The main challenge is to generalize the well-known geometric estimates given in [4, 5, 12, 14, 15, 28] to the case of embedded manifolds Γ of arbitrary codimensions. These geometric estimates rest upon suitable bounds for the closest point projection and its derivative. In the codimension-1 case, the various geometric relations between the distance function $\rho(x) \coloneqq \operatorname{dist}(x,\Gamma)$, the one-dimensional normal field $n = \nabla\rho$ and the Hessian $\mathcal{H} = \nabla \otimes \nabla\rho = \nabla n$ can be used to show that the derivative Dp of closest point projection $p(x) = x - \rho(x)n^e(x)$ is given by

$$Dp = I - n \otimes n - \rho\mathcal{H} \tag{6.1}$$

$$= P_\Gamma(I - \rho\mathcal{H}). \tag{6.2}$$

For codimension $c > 1$, such a representation cannot immediately be derived from the closest point projection when written as

$$p(x) = x - \sum_{i=1}^{c} \rho_i(x) n_i^e(x). \tag{6.3}$$

Consequently, estimates of related expressions such as derivatives of lifted and extended functions must be established by an alternative route. The route taken here is based on introducing a special tube coordinate system which is particularly well-adapted to performing computations in a tubular neighborhood of Γ, see [19, 32] for a detailed presentation and more advanced theoretical applications. Tube coordinates allow us to derive a semi-explicit representation of the derivative of the closest point projection which closely resembles the form (6.2), as well as to prove useful local trace and Poincaré-type inequalities for parts of the tubular neighborhood. After providing a short and general proof for estimating the change of the Riemannian measure when passing between discrete and continuous manifolds, we conclude this section with formulating and proving certain fat intersection properties of the discrete manifold Γ_h.

6.1. Tube Coordinates.

By the compactness of Γ and a partition of unity argument it is enough to consider a local parametrization $\alpha : \widetilde{W} \subset \mathbb{R}^d \to W \subset \Gamma \subset \mathbb{R}^k$ for which a smooth orthonormal normal frame $\{n_i\}_{i=1}^c$ exists on W. Set $B_\delta^c(0) = \{s \in \mathbb{R}^c : \|s\| < \delta\}$ and define the mapping

$$\Phi : \widetilde{W} \times B_\delta^c(0) \ni (y,s) \to \alpha(y) + \sum_{i=1}^{c} s_i n_i(\alpha(y)) \in U_\delta(\Gamma). \tag{6.4}$$

We now show that Φ actually defines a diffeomorphism by examining its derivative $D\Phi$ more closely. First, observe that $\|s\| = \rho(x)$ for $x = \Phi(y,s)$ and thus we simply write $\|s\| = \rho$. Computing $D\Phi$ gives

$$D\Phi = \begin{pmatrix} \frac{\partial \alpha_1}{\partial y_1} + \sum_{i=1}^c s_i \frac{\partial}{\partial y_1}(n_i \circ \alpha) & \dots & \frac{\partial \alpha_1}{\partial y_d} + \sum_{i=1}^c s_i \frac{\partial}{\partial y_d}(n_i \circ \alpha) & n_1^1 & \cdots & n_c^1 \\ \dots & \dots & \dots & \dots & \dots & \dots \\ \frac{\partial \alpha_k}{\partial y_1} + \sum_{i=1}^c s_i \frac{\partial}{\partial y_1}(n_i \circ \alpha) & \dots & \frac{\partial \alpha_k}{\partial y_d} + \sum_{i=1}^c s_i \frac{\partial}{\partial y_d}(n_i \circ \alpha) & n_1^k & \cdots & n_c^k \end{pmatrix} \tag{6.5}$$

$$= \underbrace{(D_y\alpha, n_1, \dots, n_c)}_{A} + \sum_{i=1}^{c} s_i \big(D_y(n_i \circ \alpha), \underbrace{0, \dots, 0}_{c \text{ zeros}}\big). \tag{6.6}$$

Clearly, the matrices $D_y(n_i \circ \alpha)$ are bounded on $\widetilde{W}$ and thus, since the columns of $D_y\alpha$ span the tangent space $T_p\Gamma$, the matrix $D\Phi$ admits a decomposition

$$D\Phi = A - \rho S, \tag{6.7}$$

with A being invertible and $\|S\|_{L^\infty(\widetilde{W})} \lesssim 1$. Consequently, for $\delta_0 < \|SA^{-1}\|_{L^\infty(\widetilde{W})}$, Φ is a local and thus also a global diffeomorphism by the bijectivity of the mapping Ψ defined in (2.6).

We recall that given a local parametrization α for Γ, the Riemannian measure $\mathrm{d}\Gamma$ is given by $\mathrm{d}\Gamma(y) = \sqrt{g^\alpha(y)}$ where $g^\alpha(y) = D_y^T\alpha(y)D_y\alpha(y)$ is the metric tensor given in local coordinates $y = (y^1, \dots, y^d)$. Rewriting $\det D\Phi = \det A \det(I - \rho S A^{-1})$ and observing that $\det(I-\rho SA^{-1}) \sim 1$ in the $\|\cdot\|_{L^\infty(\widetilde{W})}$ norm for $\delta < \delta_0$ small enough, we see that

$$\sqrt{g^\Phi(y,s)} = |\det D\Phi(y,s)| \sim |\det A| = (\det A^T A)^{\frac{1}{2}} = (\det(D^T\alpha(y)D\alpha(y))^{\frac{1}{2}} = \sqrt{g^\alpha(y)}. \quad (6.8)$$

We conclude this section by introducing a "sliced" variant of the δ-tubular neighborhood. For any d-dimensional measurable set $W \subset \Gamma \subset \mathbb{R}^k$ and $\delta < \sqrt{k}\delta_0$, we introduce the $(d+i)$-dimensional "partial cubular" neighborhood

$$Q_\delta^i(W) = \{\mathbb{R}^k \ni p + \sum_{j=1}^{i} s_j n_j(p) : p \in W \subset \Gamma \wedge \|s\|_\infty < \delta\}, \quad 0 \leqslant i \leqslant c. \quad (6.9)$$

Note that we here chose the maximum norm instead of the Euclidean norm. Clearly, $Q^c_{\sqrt{k}\delta}(\Gamma) \subset U_\delta(\Gamma) \subset Q^c_\delta(\Gamma)$. Similarly as before, we can define a parametrization Φ^i defined by

$$\Phi^i : \widetilde{W} \times Q_\delta^i(0) \ni (y,s) \to \alpha(y) + \sum_{j=1}^{i} s_j n_j(\alpha(y)) \in Q_\delta^i(W), \quad (6.10)$$

where $Q_\delta^i(0) = \{s \in \mathbb{R}^i : \|s\|_\infty < \delta\}$ is the hypercube of dimension i and length 2δ. Following the previous line of thought, we observe that for $i, j \in \{0, \dots, c\}$ and $\delta < \delta_0$ small enough

$$\sqrt{g^{\Phi^i}} \sim \sqrt{g^\alpha} \sim \sqrt{g^{\Phi^j}}. \quad (6.11)$$

Partial cubular neighborhoods will be instrumental in deriving Poincaré-type inequalities and interpolation estimates in Section 7.4 and Section 8, respectively. There, a common theme is to pass from Γ to its full tubular neighborhood $U_\delta(\Gamma)$ and vice versa by successively ascending from or descending to the i-th cubular neighborhoods Q_δ^i defined in (6.9) employing the following scaled trace and Poincaré inequalities.

Lemma 6.1. *Assume that W is an open coordinate neighborhood in Γ with a parametrization $\alpha : \widetilde{W} \to W \subset \Gamma$, $\widetilde{W} \subset \mathbb{R}^d$, and a continuously defined normal bundle. Let $w \in H^1(U_\delta^i(W))$ and $i \in \{1, \dots, c-1\}$. Then for $\delta \leqslant \delta_0$ small enough, the scaled* **trace inequality**

$$\|w\|^2_{Q_\delta^{i-1}(W)} \lesssim \delta^{-1}\|w\|^2_{Q_\delta^i(W)} + \delta\|\nabla w\|^2_{Q_\delta^i(W)}, \quad (6.12)$$

holds as well as the scaled **Poincaré inequality**

$$\|w\|^2_{Q_\delta^i(W)} \lesssim \delta\|w\|^2_{Q_\delta^{i-1}(W)} + \delta^2\|\nabla w\|^2_{Q_\delta^i(W)}. \quad (6.13)$$

Proof. We start with the proof for trace inequality (6.12). By a density argument, it is enough to assume that $w \in C^1(Q_\delta^i(W))$. Rewrite the integral $\|w\|^2_{Q_\delta^{i-1}(W)}$ using the tube coordinates (6.10) and the measure equivalence (6.11) to see that

$$\|w\|^2_{Q_\delta^i(W)} = \int_{\widetilde{W}} \left(\int_{Q_\delta^i(0)} |w(y,s)|^2 \sqrt{g^{\Phi_i}(y,s)}\,\mathrm{d}s \right) \mathrm{d}y \sim \int_{\widetilde{W}} \left(\int_{Q_\delta^i(0)} |w(y,s)|^2\,\mathrm{d}s \right) \sqrt{g^\alpha(y)}\,\mathrm{d}y, \quad (6.14)$$

Fixing y, the fundamental theorem of calculus allows us to rewrite the integrand $v(s) = w(y,s)$ as

$$v(s_1, \dots, s_i) = v(s_1, \dots, s_{i-1}, 0) + \int_0^{s_i} \partial_{s_i} v(s_1, \dots, s_{i-1}, s)\,\mathrm{d}s_i, \quad (6.15)$$

and consequently, after rearranging terms and a Cauchy-Schwarz inequality,

$$|v(s_1, \dots, s_{i-1}, 0)|^2 \lesssim |v(s)|^2 + \left(\int_{-\delta}^{\delta} |\partial_{s_i} v(s_1, \dots, s_{i-1}, s_i)|\,\mathrm{d}s_i \right)^2 \quad (6.16)$$

$$\lesssim |v(s)|^2 + \delta \int_{-\delta}^{\delta} |\partial_{s_i} v(s_1, \dots, s_{i-1}, s_i)|^2\,\mathrm{d}s_i. \quad (6.17)$$

Integrating the previous inequality over $Q_\delta^i(0)$ gives

$$\delta \int_{Q_\delta^{i-1}(0)} |v(s_1,\dots,s_{i-1},0)|^2 ds \lesssim \int_{Q_\delta^i(0)} |v(s)|^2 ds + \delta^2 \int_{Q_\delta^i(0)} |\partial_{s_i} v(s)|^2 \,\mathrm{d}s, \tag{6.18}$$

and a subsequent integration over $\widetilde{W}$ together with equivalence (6.14) finally leads us to

$$\delta \|w\|^2_{Q_\delta^{i-1}(W)} \lesssim \|w\|^2_{Q_\delta^i(W)} + \delta^2 \|\nabla w\|^2_{Q_\delta^i(W)}. \tag{6.19}$$

Finally, observe that starting from the representation (6.15) and rearranging terms properly, the Poincaré inequality (6.13) can be proven in the exact same manner. □

6.2. **Gradient of Lifted and Extended Functions.** Next, using tube coordinates, we derive a semi-explicit representation of the derivative of the closest point projection.

Lemma 6.2. *Whenever $\delta \leqslant \delta_0$ for δ_0 small enough, the derivative Dp of the closest point projection $p : U_\delta(\Gamma) \to \Gamma$ admits a representation of the form*

$$Dp = P_\Gamma(I - \rho\mathcal{H}), \tag{6.20}$$

with a matrix-valued function $\mathcal{H}$ satisfying $\|\mathcal{H}\|_{L^\infty(U_\delta(\Gamma))} \lesssim 1$ and $\mathcal{H}P_\Gamma = \mathcal{H}$.

Proof. Using local tube coordinates (6.4), we observe that the closest point projection p can be written as

$$U_\delta(\Gamma) \ni x \mapsto p(x) = \alpha \circ \wp \circ \Phi^{-1}(x), \tag{6.21}$$

where $\wp : \mathbb{R}^k \to \mathbb{R}^d$ is the linear projection on the first d components, i.e., $\wp(y,s) = y$ for $(y,s) \in \mathbb{R}^d \times \mathbb{R}^c$. Since $\wp$ is the linear projection on the first d components, its total derivative at (y,s) applied to a (tangent) vector $w \in \mathbb{R}^k$ is simply $D\wp(y,s)w = [\boldsymbol{I}_{d\times d}, \mathbf{0}_{d\times c}]w$. Writing $(y,s) = \Phi^{-1}(x)$ and applying the chain rule shows that the total derivative of p at $x \in U_\delta(\Gamma)$ can be computed by

$$Dp(x) = D\alpha(\wp(y,s))[\boldsymbol{I}_{d\times d}, \mathbf{0}_{d\times c}](D\Phi^{-1})(x). \tag{6.22}$$

Then starting from the matrix decomposition $D\Phi(y,s) = A(y,s) - \rho S(y,s)$ derived in the previous section, we insert a power series representation for the inverse matrix $(A-\rho S)^{-1} = A^{-1}(I - \rho S A^{-1})^{-1}$ into $D\Phi^{-1}(x) = (D\Phi(y,s))^{-1}$ and conclude that (omitting function arguments)

$$Dp = D\alpha[\boldsymbol{I}_{d\times d}, \mathbf{0}_{d\times c}]A^{-1}(I + \rho \sum_{l=1}^{\infty} \rho^{l-1}(SA^{-1})^l), \tag{6.23}$$

$$= D\alpha[\boldsymbol{I}_{d\times d}, \mathbf{0}_{d\times c}]A^{-1}(I - \rho\mathcal{H}), \tag{6.24}$$

with the absolutely and uniformly convergent power series $\mathcal{H} = -\sum_{l=1}^{\infty} \rho^{l-1}(SA^{-1})^l$. To arrive at representation (6.20), it remains to show that

$$D\alpha[\boldsymbol{I}_{d\times d}, \mathbf{0}_{d\times c}]A^{-1} = P_\Gamma. \tag{6.25}$$

Setting $w = A^{-1}v$, and recalling the definition of A from (6.6), a simple computation yields

$$D\alpha[\boldsymbol{I}_{d\times d}, \mathbf{0}_{d\times c}]A^{-1}v = D\alpha(w_1,\dots w_d) = P_\Gamma[D\alpha, n_1, \dots, n_c]w = P_\Gamma A w = P_\Gamma v \tag{6.26}$$

for any $v \in \mathbb{R}^k$ since $P_\Gamma(\partial_i \alpha) = \partial_i \alpha$ and $P_\Gamma(n_i) = 0$. Finally, we demonstrate that $\mathcal{H}P_\Gamma = \mathcal{H}$, or equivalently, that $\mathcal{H}n_i = 0$ for $i = 1,\dots,c$. Referring back to (6.6), we see that SA^{-1} consists of a (weighted) sum of matrices of the form

$$[D_y(n_i \circ \alpha), 0, \dots, 0)]A^{-1} = D_y(n_i \circ \alpha)[\boldsymbol{I}_{d\times d}, \mathbf{0}_{d\times c}]A^{-1} \tag{6.27}$$

$$= D_x n_i(\alpha(\cdot)) D_y \alpha[\boldsymbol{I}_{d\times d}, \mathbf{0}_{d\times c}]A^{-1} \tag{6.28}$$

$$= D_x n_i(\alpha(\cdot)) P_\Gamma, \tag{6.29}$$

thanks to (6.25) and thus $\mathcal{H}P_\Gamma = \mathcal{H}$ which concludes the proof. □

Based on the previous lemma, estimates for the gradient of lifted and extended functions can be established. Starting from $Dv^e = Dv \circ Dp$ and the definition of the gradient as the (point-wise) Riesz representation of the total derivative Dv^e with respect to the standard Euclidean scalar product $\langle \cdot, \cdot \rangle_{\mathbb{R}^k}$, we conclude that $\forall\, a \in \mathbb{R}^k$

$$\langle \nabla v^e, a \rangle_{\mathbb{R}^k} = (Dv \circ Dp)a = Dv P_\Gamma (I - \rho \mathcal{H})a = \langle (I - \rho \mathcal{H}^T) P_\Gamma \nabla v, a \rangle_{\mathbb{R}^k} \tag{6.30}$$

and thus

$$\nabla v^e = (I - \rho \mathcal{H}^T) P_\Gamma \nabla v = (I - \rho \mathcal{H}^T) \nabla_\Gamma v = P_\Gamma (I - \rho \mathcal{H}^T) \nabla_\Gamma v, \tag{6.31}$$

$$\nabla_{\Gamma_h} v^e = P_{\Gamma_h} (I - \rho \mathcal{H}^T) P_\Gamma \nabla v = B^T \nabla_\Gamma v, \tag{6.32}$$

where the invertible linear mapping

$$B = P_\Gamma (I - \rho H) P_{\Gamma_h} : T_x(\Gamma_h) \to T_{p(x)}(\Gamma) \tag{6.33}$$

maps the tangent space of Γ_h at x to the tangent space of Γ at $p(x)$. Setting $v = w^l$ and using the identity $(w^l)^e = w$, we immediately get that

$$\nabla_\Gamma w^l = B^{-T} \nabla_{\Gamma_h} w \tag{6.34}$$

for any elementwise differentiable function w on Γ_h lifted to Γ. Similar to the standard hypersurface case $d = k - 1$ in [14, 15], the following bounds for the linear operator B can be derived.

Lemma 6.3. *It holds*

$$\|B\|_{L^\infty(\Gamma_h)} \lesssim 1, \quad \|B^{-1}\|_{L^\infty(\Gamma)} \lesssim 1, \quad \|P_\Gamma - BB^T\|_{L^\infty(\Gamma)} \lesssim h^2. \tag{6.35}$$

Proof. Thanks to the representation (6.20), the proof follows standard arguments, see Dziuk and Elliott [15], and is only sketched here for completeness. The first two bounds follow directly from Lemma 6.2. Using the assumption $\|\rho\|_{L^\infty(\Gamma_h)} \lesssim h^2$, it follows that $P_\Gamma - BB^T = P_\Gamma - P_\Gamma P_{\Gamma_h} P_\Gamma + O(h^2)$. An easy calculation now shows that $P_\Gamma - P_\Gamma P_{\Gamma_h} P_\Gamma = P_\Gamma (P_\Gamma - P_{\Gamma_h})^2 P_\Gamma$ from which the desired bound follows by observing that

$$P_\Gamma - P_{\Gamma_h} = \sum_{i=1}^{d} \big((t_i - t_i^h) \otimes t_i + t_i^h \otimes (t_i - t_i^h) \big) \tag{6.36}$$

and thus $\|(P_\Gamma - P_{\Gamma_h})^2\|_{L^\infty(\Gamma_h)} \lesssim \sum_{i=1}^d \|t_i - t_i^h\|^2_{L^\infty(\Gamma_h)} \lesssim h^2$. □

To estimate the quadrature error for the full gradient form a_h^2 as defined in Table 1, we will need to quantify the error introduced by using the full gradient ∇ in (3.16) instead of ∇_{Γ_h}. To do so, we decompose the full gradient as $\nabla = \nabla_{\Gamma_h} + Q_{\Gamma_h} \nabla$. An estimate for the normal component is provided by the following Lemma.

Lemma 6.4. *For $v \in H^1(\Gamma)$ it holds*

$$\|Q_{\Gamma_h} \nabla v^e\|_\Gamma \lesssim h \|\nabla_\Gamma v\|_\Gamma. \tag{6.37}$$

Proof. Since $\nabla v^e = P_\Gamma (I - \rho \mathcal{H}^T) \nabla_\Gamma v$ according to identity (6.31), it is enough to prove that

$$\|Q_{\Gamma_h} P_\Gamma\|_{L^\infty(\Gamma)} \lesssim h. \tag{6.38}$$

But using representation (2.3) and (2.4), a simple computation shows that

$$\|Q_{\Gamma_h} P_\Gamma\|_{L^\infty(\Gamma)} \leqslant \sum_{i=1}^{c} \|n_i^h \otimes n_i^h - \langle n_i^h, n_i \rangle n_i^h \otimes n_i\|_{L^\infty(\Gamma)} \tag{6.39}$$

$$\leqslant \sum_{i=1}^{c} \big(\|(1 - \langle n_i^h, n_i \rangle) n_i^h \otimes n_i^h\|_{L^\infty(\Gamma)} + \|\langle n_i^h, n_i \rangle n_i^h \otimes (n_i - n_i^h)\|_{L^\infty(\Gamma)} \big) \tag{6.40}$$

$$\lesssim h^2 + h, \tag{6.41}$$

where we used the identity $1 - \langle n_i^h, n_i \rangle = \frac{1}{2} \langle n_i^h - n_i, n_i^h - n_i \rangle$ and approximation assumption (3.4). □

6.3. **Change of Domain of Integration.** Next, we derive estimates for the change of the Riemannian measure when integrals are lifted from the discrete surface to the continuous surface and vice versa. For a subset $\omega \subset \Gamma_h$, we have the change of variables formulas

$$\int_{\omega^l} g^l \,\mathrm{d}\Gamma = \int_{\omega} g|B|_d \,\mathrm{d}\Gamma_h, \tag{6.42}$$

with $|B|_d$ denoting the absolute value of the determinant of B. The determinant $|B|_d$ satisfies the following estimate

Lemma 6.5. *It holds*

$$\|1 - |B|_d\|_{L^\infty(\Gamma_h)} \lesssim h^2, \qquad \||B|_d\|_{L^\infty(\Gamma_h)} \lesssim 1, \qquad \||B|_d^{-1}\|_{L^\infty(\Gamma_h)} \lesssim 1. \tag{6.43}$$

Proof. See [11, 12] and [4] for a proof in the case of $d = k - 1$. Recall that given a Riemannian metric on a d-dimensional manifold Γ, the canonical measure $\mathrm{d}\Gamma$ on Γ is defined by the unique volume form ω_Γ satisfying $\omega_\Gamma(e_1, \dots, e_d) = 1$ for one (and hence any) orthonormal frame $\{e_i\}_{i=1}^d$ on the tangent bundle $T\Gamma$. Writing $\mathrm{d}\Gamma = \omega_\Gamma$, the volume form is given by the pullback

$$\mathrm{d}\Gamma = i^*(e^1 \wedge \ldots \wedge e^d), \tag{6.44}$$

i.e., the restriction to Γ of the d-form defined by the outer product of the dual coframe $\{e^i\}_{i=1}^d$ satisfying $e^i(e_j) = \langle e_i, e_j\rangle = \delta^i_j$. Here, $i : \Gamma \hookrightarrow \mathbb{R}^k$ denotes the inclusion of Γ into $\mathbb{R}^k$ given by the identity map. Thanks to the evaluation formula

$$(e^1 \wedge \ldots \wedge e^d)(v_1, \dots, v_k) = \det((e^i(v_j)) = \det(\langle e_i, v_j\rangle), \tag{6.45}$$

the defined form $\mathrm{d}\Gamma$ clearly satisfies $\mathrm{d}\Gamma(e_1, \dots, e_d) = 1$. Now the pull-backed volume form $p^*\,\mathrm{d}\Gamma$ is described in terms of the volume form $\mathrm{d}\Gamma_h$ by the identity $p^*\,\mathrm{d}\Gamma = |B|_d\,\mathrm{d}\Gamma_h$, where $|B|_d$ is determinant of B as a linear mapping $B : T_xK \to T_{p(x)}\Gamma$ and $\mathrm{d}\Gamma_h$ denotes the canonical volume form defined on Γ_h. Thus we have the transformation rule $\int_{K^l} f\,\mathrm{d}\Gamma = \int_K p^*(f\,\mathrm{d}\Gamma) = \int_K f^e|B|_d\,\mathrm{d}\Gamma_h$. Taking an orthonormal tangential frame $\{e_i^h\}_{i=1}^d$ of $T\Gamma_h$, the determinant $|B|_d$ can be simply computed by

$$|B|_d = p^*\,\mathrm{d}\Gamma(e_1^h, \dots, e_d^h) = \mathrm{d}\Gamma(Dpe_1^h, \dots, Dpe_d^h) = \det(\langle e_i, Dpe_j^h\rangle). \tag{6.46}$$

Next, observe that the representation (6.20) of Dp yields $\langle e_i, Dpe_j^h\rangle = \langle e_i, P_\Gamma e_j^h\rangle + O(h^2) = \langle e_i, e_j^h\rangle + O(h^2)$. Moreover, for $i = j$, one has $2(1 - \langle e_i, e_i^h\rangle) = \langle e_i - e_i^h, e_i - e_i^h\rangle \lesssim h^2$ while for $i \neq j$, $\langle e_i, e_j^h\rangle = \langle e_i, e_j^h - e_j\rangle \lesssim h$. Consequently,

$$\det(\langle e_i, Dpe_j^h\rangle) = \det(a_{ij}) \qquad \text{with } a_{ij} = \begin{cases} 1 + O(h^2) & \text{if } i = j, \\ O(h) & \text{else.} \end{cases} \tag{6.47}$$

Recalling the definition of the determinant $\det(a_{ij}) = \sum_{\sigma\in S(d)} \mathrm{sig}(\sigma)\Pi_{i=1}^d a_{i\sigma(i)}$ and examining the product for a single permutation $\sigma \in S(d)$ we see that

$$\Pi_{i=1}^d a_{i\sigma(i)} = \begin{cases} (1 + O(h^2))^d & \text{if } \sigma = \mathrm{Id}, \\ O(h^2) & \text{else,} \end{cases} \tag{6.48}$$

since any other permutation than the identity involves at least two non-diagonal elements. Hence $|B|_d = 1 + O(h^2)$. ∎

We conclude this section by noting that combining the estimates (6.35) and (6.43) for respectively the norm and the determinant of B shows that for $m = 0, 1$

$$\|v\|_{H^m(\mathcal{K}_h^l)} \sim \|v^e\|_{H^m(\mathcal{K}_h)} \quad \text{for } v \in H^m(\mathcal{K}_h^l), \tag{6.49}$$

$$\|w^l\|_{H^m(\mathcal{K}_h^l)} \sim \|w\|_{H^m(\mathcal{K}_h)} \quad \text{for } w \in V_h. \tag{6.50}$$

6.4. **Fat Intersection Covering.** Since the manifold geometry is embedded into a fixed background mesh, the active mesh $\mathcal{T}_h$ might contain elements which barely intersect the discretized manifold Γ_h. Such "small cut elements" typically prohibit the application of a whole set of well-known estimates, such as interpolation estimates and inverse inequalities, which typically rely on certain scaling properties. As a partial replacement for the lost scaling properties we here recall from [4] the concept of *fat intersection coverings* of $\mathcal{T}_h$.

In Burman et al. [4] it was proved that the active mesh fulfills a fat intersection property which roughly states that for every element there is a close-by element which has a significant intersection with Γ_h. More precisely, let x be a point on Γ and let $B_\delta(x) = \{y \in \mathbb{R}^k : |x-y| < \delta\}$ and $D_\delta = B_\delta(x) \cap \Gamma$. We define the sets of elements

$$\mathcal{K}_{\delta,x} = \{K \in \mathcal{K}_h : \overline{K}^l \cap D_\delta(x) \neq \emptyset\}, \qquad \mathcal{T}_{\delta,x} = \{T \in \mathcal{T}_h : T \cap \Gamma_h \in \mathcal{K}_{\delta,x}\}. \tag{6.51}$$

With $\delta \sim h$ we use the notation $\mathcal{K}_{h,x}$ and $\mathcal{T}_{h,x}$. For each $\mathcal{T}_h$, $h \in (0, h_0]$ there is a set of points $\mathcal{X}_h$ on Γ such that $\{\mathcal{K}_{h,x}, x \in \mathcal{X}_h\}$ and $\{\mathcal{T}_{h,x}, x \in \mathcal{X}_h\}$ are coverings of $\mathcal{T}_h$ and $\mathcal{K}_h$ with the following properties:

- The number of sets containing a given point y is uniformly bounded
$$\#\{x \in \mathcal{X}_h : y \in \mathcal{T}_{h,x}\} \lesssim 1 \quad \forall\, y \in \mathbb{R}^k \tag{6.52}$$
for all $h \in (0, h_0]$ with h_0 small enough.
- The number of elements in the sets $\mathcal{T}_{h,x}$ is uniformly bounded
$$\#\mathcal{T}_{h,x} \lesssim 1 \quad \forall\, x \in \mathcal{X}_h \tag{6.53}$$
for all $h \in (0, h_0]$ with h_0 small enough, and each element in $\mathcal{T}_{h,x}$ shares at least one face with another element in $\mathcal{T}_{h,x}$.
- $\forall\, h \in (0, h_0]$ with h_0 small enough, and $\forall\, x \in \mathcal{X}_h$, $\exists T_x \in \mathcal{T}_{h,x}$ that has a large (fat) intersection with Γ_h in the sense that
$$|T_x| \sim h^c |T_x \cap \Gamma_h| = h^c |K_x| \quad \forall\, x \in \mathcal{X}_h. \tag{6.54}$$

These properties basically guarantee that any quasi-uniform mesh $\mathcal{T}^h$ with $h \leqslant h_0$ resolves Γ_h sufficiently. While the proof in [4] was only concerned with the surface case $d = k-1$, it directly transfers to the case of arbitrary codimensions.

6.5. **Fat Intersection Property for the Discrete Normal Tube.** The goal of this section is to present a refined version of the fat intersection covering, roughly stating that a significant portion of each element can be reached from the discrete manifold Γ_h by walking along normal-like paths which reside completely inside $\mathcal{T}_h$. We will need the following notation.

- Let $T \in \mathcal{T}_h$ and let $\mathcal{N}(T) = \{\widetilde{T} \in \mathcal{T}_h : T \cap \widetilde{T} \neq \emptyset\} \subset \mathcal{T}_h$ denote the set consisting of T and all its neighbors that also belongs to the active mesh $\mathcal{T}_h$.
- Let x be a vertex of an element $T \in \widetilde{\mathcal{T}}_h$ then the star $\mathcal{S}(x)$ is the set of *all* elements in the background mesh $\widetilde{\mathcal{T}}_h$ that share the vertex x.

Lemma 6.6. *For each $T \in \mathcal{T}_h$ there is a d-dimensional plane $\overline{\Gamma} = \overline{\Gamma}_T$ with constant normal bundle $\{\overline{n}_i\}_{i=1}^c = \{\overline{n}_{i,T}\}_{i=1}^c$ satisfying the geometry approximation assumptions*

$$\Gamma_h \cap \mathcal{N}(T) \subset U_\epsilon(\overline{\Gamma}), \qquad \sup_{T \in \mathcal{T}_h} \|\overline{n}_{i,T} - n_i\|_{L^\infty(\mathcal{N}(T))} \lesssim h \quad \text{for } i = 1, \dots, c, \tag{6.55}$$

with $\epsilon \sim h^2$. Furthermore, $\Gamma_h \cap \mathcal{N}(T)$ is a Lipschitz function over $\overline{\Gamma}$ and its Lipschitz constant is uniformly bounded over all $T \in \mathcal{T}_h$.

Proof. To verify (6.55) we take $x \in p(\mathcal{N}(T)) \subset \Gamma$ and let $\overline{\Gamma}_T$ be the tangent plane to Γ at x. Next we note that by the geometry approximation assumptions we have $\Gamma_h \subset U_{\delta'}(\Gamma)$ with $\delta' \sim h^2$. Now let $B_\delta(x)$ be a ball of radius $\delta \sim h$ such that $\mathcal{N}(T) \subset B_\delta(x)$ and $p(\mathcal{N}(T)) \subset B_\delta(x)$. Using the smoothness of Γ and the fact that $\overline{\Gamma}$ is the tangent plane to Γ at x we find that there is $\delta'' \sim h^2$ such that

$$\Gamma_h \cap \mathcal{N}(T) \subset \Gamma_h \cap B_\delta(x) \subset U_{\delta'}(\Gamma) \cap B_\delta(x) \subset U_{\delta''}(\overline{\Gamma}). \tag{6.56}$$

Finally, we note that choosing $\overline{n}_i = n_i(x)$, the smoothness assumptions on Γ together with the geometric approximation assumption (3.4) yields $\|\overline{n}_i - n_i(y)\|_{\mathbb{R}^k} = \|n_i(x) - n_i(y)\|_{\mathbb{R}^k} \lesssim \delta \sim h$ for $y \in B_\delta(x)$. □

Next, we introduce some notation to describe normal-like paths given by projecting sets into Γ_h.

- Let ω be a set and x a point then the cone with base ω and vertex z is defined by
$$\mathrm{Cone}(\omega, z) = \bigcup_{x\in\omega} I(z, x), \tag{6.57}$$
where $I(z, x)$ is the line segment with endpoints x and x.
- Let $\overline{p}_h$ be the mapping onto Γ_h obtained by following a unique normal direction $\overline{n} \in \mathrm{span}\{\overline{n}_1, \dots, \overline{n}_c\}$ from x to Γ_h. Given a set ω we define the cylinder over Γ_h by
$$\mathrm{Cyl}(\omega, \Gamma_h) = \bigcup_{x\in\omega} I(x, \overline{p}_h(x)). \tag{6.58}$$

With this notation we can formulate and prove the following Lemma.

Lemma 6.7. *For each $T \in \mathcal{T}_h$ there is a ball $B_\delta \subset T$ with radius $\delta \sim h$ such that*
$$\mathit{Cyl}(B_\delta, \Gamma_h) \subset \mathcal{N}(T). \tag{6.59}$$

Proof. To keep the mathematical technicalities at a moderate level, we restrict ourselves to the most important case $c = 1$. For $T \in \mathcal{T}_h$, let R_T be the radius of the circumscribed sphere of element T and r_T the radius of the inscribed sphere in T. The center of the inscribed sphere is denoted by x_T. We recall that the element is shape regular which means that $r_T \sim R_T \sim h$. Let $\{x_i\}_{i=0}^k$ be the vertices of T, then by shape regularity there is $\delta_1 \sim h$ such that the ball $B_{\delta_1}(x_i) \subset \mathcal{S}(x_i)$ for each i. For technical reasons we will also choose δ_1 such that
$$\delta_1 \leq \min_{i=\in\{0,\dots,k\}} \|x_i - x_T\|_{\mathbb{R}^k}, \tag{6.60}$$
where x_T is the center of the inscribed sphere. By shape regularity it follows that $r_T \leq \delta_i \leq R_T$, $i = 0, \dots, k$ and thus we may still take $\delta_1 \gtrsim h$. To prove (6.59), we consider two different intersection cases, see also Figure 2.

Intersection Case *I*. Assume that
$$\overline{\Gamma} \cap T \subset T \setminus \left(\bigcup_{i=0}^k B_{\delta_1/8}(x_i) \right), \tag{6.61}$$
then we shall construct a ball $B_{\delta_2}(x) \subset T$ with $x \in \overline{\Gamma} \cap T$, and $\delta_2 \sim h$. We note that $\overline{\Gamma}$ must intersect at least one of the $k+1$ line segments $I(x_T, x_i)$ that join x_T with the nodes x_i, say the line segment from x_T to x_0, and that there is an intersection point $z = I(x_T, x_0) \cap \Gamma_h$ such that
$$\delta_1/8 \leq \|z - x_0\|_{\mathbb{R}^k}. \tag{6.62}$$
We note that $\mathrm{Cone}(B_{r_T}(x_T), x_0) \subset T$ and that $B_{\delta_2}(z) \subset \mathrm{Cone}(B_{r_T}(x_T), x_0)$ where
$$\delta_2 = r_T \frac{\|z - x_T\|_{\mathbb{R}^k}}{\|x_0 - x_T\|_{\mathbb{R}^k}} \tag{6.63}$$
is a suitable scaling of r_T. We also note that $\delta_2 \sim h$ since
$$\delta_2 = r_T \frac{\|z - x_T\|_{\mathbb{R}^k}}{\|x_0 - x_T\|_{\mathbb{R}^k}} \geq \frac{r_T}{2} \frac{\|x_0 - x_T\|_{\mathbb{R}^k} - \delta_1/8 + 2\epsilon}{\|x_0 - x_T\|_{\mathbb{R}^k}} \tag{6.64}$$
$$\geq \frac{r_T}{2} \left(1 - \frac{\delta_1}{8 \underbrace{\|x_0 - x_T\|_{\mathbb{R}^k}}_{\geq \delta_1}} \right) \geq r_T \frac{7}{16} \sim h. \tag{6.65}$$
We finally note that for ϵ/δ_1 small enough we clearly have
$$\mathrm{Cyl}(B_{\delta_2/2}(z), \Gamma_h) \subset B_{\delta_2}(z) \subset T. \tag{6.66}$$

Intersection Case *II*. There is at least one i, say $i = 0$, such that

$$B_{\delta_1/8}(x_0) \cap \overline{\Gamma} \neq \emptyset. \tag{6.67}$$

We divide this case in two subcases

$$\begin{cases} B_{r_T/2}(x_T) \cap \overline{\Gamma} \neq \emptyset & \text{Case } II_1, \\ B_{r_T/2}(x_T) \cap \overline{\Gamma} = \emptyset & \text{Case } II_2. \end{cases} \tag{6.68}$$

Case II_1. Let z be the point on $\overline{\Gamma}$ with minimal distance to x_T, we then have $\|z - x_T\|_{\mathbb{R}^k} \leq r_T/2$, and $B_{r_T/2}(z) \subset B_{r_T}(x_T)$. Then we conclude that

$$\mathrm{Cyl}(B_{r_T/4}(z), \Gamma_h) \subset B_{r_T/2}(z) \subset T \tag{6.69}$$

for ϵ/r_T small enough.
Case II_2. Consider the ball $B_{\delta_1}(x_0) \subset \mathcal{S}(x_0)$, and observe that we have a partition

$$B_{\delta_1}(x_0) = B^+_{\delta_1}(x_0) \cup (B_{\delta_1}(x_0) \cap \Gamma_h) \cup B^-_{\delta_1}(x_0), \tag{6.70}$$

where $B^{\pm}_{\delta_1}(x_0)$ are the two connected components of $B_{\delta_1}(x_0) \setminus \Gamma_h$. Without loss of generality we may assume that $x_0 \in (B_{\delta_1}(x_0) \cap \Gamma_h) \cup B^-_{\delta_1}(x_0)$. Then we have

$$B^+_{\delta_1}(x_0) \subset \mathcal{S}(x_0) \cap \mathcal{N}(T) \subset \mathcal{N}(T). \tag{6.71}$$

To verify (6.71) we note that if $x_0 \in \Gamma_h$ we have $B^+_{\delta_1}(x_0) \subset B_{\delta_1}(x_0) \subset \mathcal{S}(x_0) \subset \mathcal{N}(T)$. Next, if $x_0 \in B^-_{\delta_1}(x_0)$ we instead note that an element T' in $\mathcal{S}(x_0)$ which does not belong to $\mathcal{T}_h$ must satisfy $T' \cap B_{\delta_1}(x_0) \subset B^-_{\delta_1}(x_0)$ and thus we conclude that all elements in $\mathcal{S}(x_0)$ that intersect $B^+_{\delta_1}(x_0)$ must be in the active mesh $\mathcal{T}_h$. We therefore have $B^+_{\delta_1}(x_0) \subset \mathcal{S}(x_0) \cap \mathcal{T}_h$ which concludes the verification of (6.71).

Next we note that it follows from the assumptions in Case II_1 that for ϵ/r_T small enough it holds $B_{r_T/2-2\epsilon} \cap U_\epsilon(\overline{\Gamma}) = \emptyset$, $B_{r_T/4}(x_T) \subset B_{r_T/2-2\epsilon}$ and thus in particular $B_{r_T/4}(x_T) \cap U_\epsilon(\overline{\Gamma}) = \emptyset$, and

$$\big(B_{\delta_1}(x_0) \setminus B_{\delta_1/8+\epsilon}(x_0)\big) \cap \mathrm{Cone}(B_{r_T/4}(x_T), x_0) \subset B^+_{\delta_1}(x_0). \tag{6.72}$$

For ϵ/δ_1 small enough we have $B_{\delta_1/8+\epsilon}(x_0) \subset B_{\delta_1/4}(x_0)$ and may in the same way as in Case I construct a ball $B_{\delta_3}(z)$, with z on $I(x_0, x_T)$ and $\delta_3 \sim h$ such that

$$B_{\delta_3}(z) \subset \big(B_{\delta_1/2}(x_0) \setminus B_{\delta_1/4}(x_0)\big) \cap \mathrm{Cone}(B_{r_T/4}(x_T), x_0) \subset B^+_{\delta_1}(x_0). \tag{6.73}$$

Then, for ϵ/δ_1 small enough the cylinder $\mathrm{Cyl}(B_{\delta_3}, \Gamma_h)$ satisfies

$$\mathrm{Cyl}(B_{\delta_3}, \Gamma_h) \subset B^+_{\delta_1}(x_0) \subset \mathcal{N}(T), \tag{6.74}$$

which concludes the proof. □

7. Verification of the Inverse and Discrete Poincaré Estimates

We now show that any combination of discrete bilinear forms a_h and stabilization forms s_h from Table 1 in Section 3.3 yields a stabilized cut finite element formulation which satisfies both the discrete Poincaré estimate (4.1) and the inverse estimate (4.2). The core idea behind the forthcoming proofs of the discrete Poincaré estimates is to show that a properly scaled L^2 norm of a discrete function $v \in V_h$ computed on $\mathcal{T}_h$ can be controlled by the L^2 norm on the discrete manifold Γ_h augmented by the stabilization form in question,

$$\|v\|^2_{\mathcal{T}_h} \lesssim h^c \|v\|^2_{\Gamma_h} + s_h(v, v) \quad \forall\, v \in \mathcal{V}_h. \tag{7.1}$$

Then the desired discrete Poincaré estimate follows directly from estimating $\|v\|_{\Gamma_h}$ using the Γ_h-based, continuous Poincaré inequality stated and proved in [4, Lemma 4.1]:

Lemma 7.1. *For $v \in H^1(\Gamma_h)$, the following estimate holds*

$$\|v - \lambda_{\Gamma_h}(v)\|_{\Gamma_h} \lesssim \|\nabla_{\Gamma_h} v\|_{\Gamma_h} \tag{7.2}$$

for $0 < h \leq h_0$ with h_0 small enough.

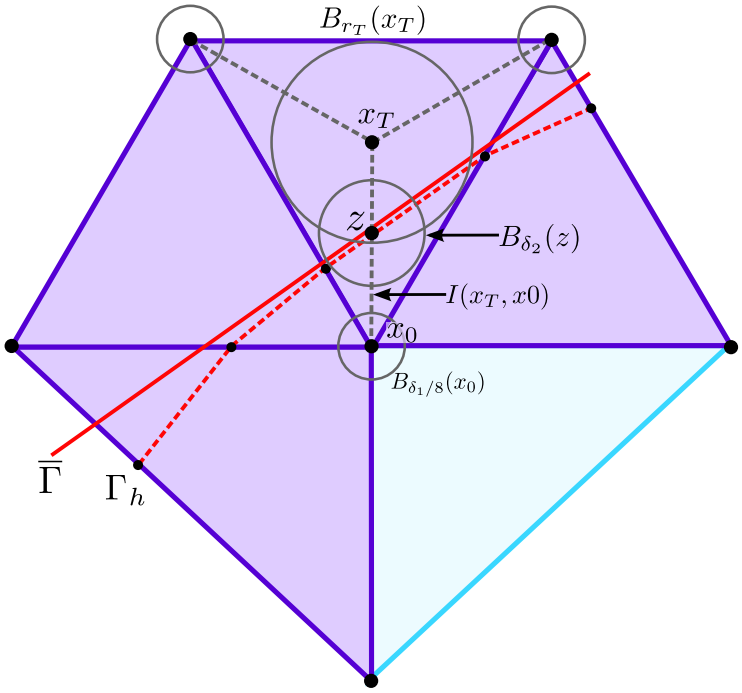

(A) Intersection case I.

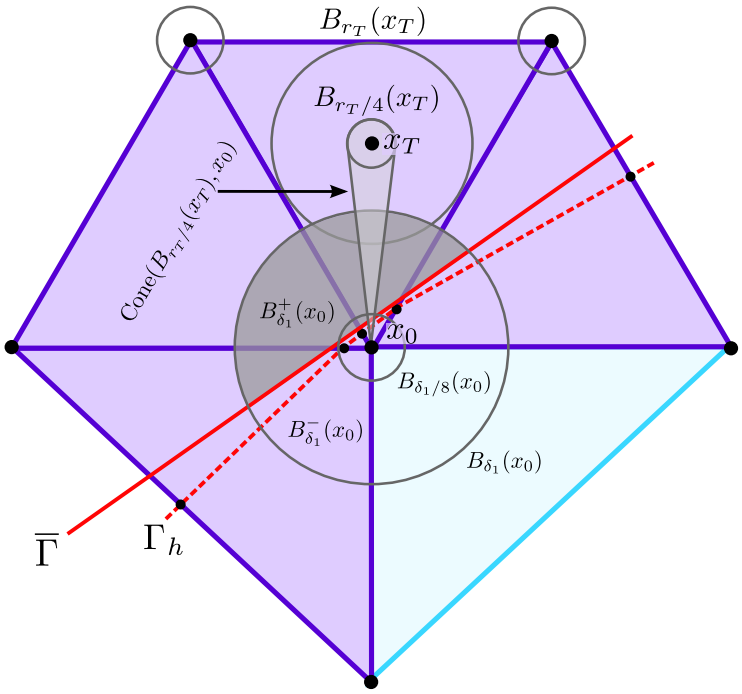

(B) Intersection case IIb.

FIGURE 2. Schematic drawing of the two intersection cases I and IIb in the proof of Lemma 6.7.

An inspection of the short proof given in [4] shows that the result (7.2) holds for any codimension. The forthcoming proofs of (7.1) will also make use of various inverse estimates which we state next.

7.1. **Inverse Estimates.** Recall that for given $T \in \mathcal{T}_h$, the following well-known inverse estimates hold for $v_h \in V_h$:

$$\|\nabla v_h\|_T \lesssim h^{-1}\|v_h\|_T, \qquad \|v_h\|_{\partial T} \lesssim h^{-1/2}\|v_h\|_T, \qquad \|\nabla v_h\|_{\partial T} \lesssim h^{-1/2}\|\nabla v_h\|_T. \tag{7.3}$$

In addition, in the course of our analysis, we will also employ "cut versions" of these inverse estimates as specified in

Lemma 7.2. *Let $K \in \mathcal{K}_h$ and $T \in \mathcal{T}_h$, then*

$$h^c\|v_h\|^2_{K\cap T} \lesssim \|v_h\|^2_T, \qquad h^c\|\nabla v_h\|^2_{K\cap T} \lesssim \|\nabla v_h\|^2_T. \tag{7.4}$$

Proof. Recalling that the mesh is supposed to be shape regular and labeling finite element functions and sets defined on the standard reference element with $\widehat{\cdot}$, the proof follows immediately from a standard scaling and finite dimensionality argument leading to the following chain of estimates

$$\|v_h\|^2_{K\cap T} \lesssim h^d\|\widehat{v}_h\|^2_{\widehat{K}\cap\widehat{T}} \lesssim h^d\|\widehat{v}_h\|^2_{L^\infty(\widehat{T})}\underbrace{|\widehat{K}\cap\widehat{T}|}_{\lesssim 1} \lesssim h^d\|\widehat{v}_h\|^2_{\widehat{T}} \lesssim h^{d-k}\|v_h\|^2_T, \tag{7.5}$$

which is precisely the first inequality in (7.4). Note that the hidden constant in $|\widehat{K}\cap\widehat{T}| \lesssim 1$ ultimately depends on the curvature of Γ. The second one can be derived analogously. □

Now the verification of the abstract inverse estimate (4.2) for any combination of discrete bilinear forms a_h^i and stabilizations s_h^i defined in Table 1 is a simple consequence of the following lemma.

Lemma 7.3. *Let $v \in V_{h,0}$ then the following inverse estimate holds*

$$\|v\|^2_{a_h^i} \lesssim h^{-2-c}\|v\|^2_{\mathcal{T}_h} \quad i = 1, 2, \tag{7.6}$$

$$\|v\|^2_{s_h^1} \lesssim h^{-2-c}\|v\|^2_{\mathcal{T}_h}, \qquad \|v\|^2_{s_h^2} \lesssim h^{-c}\|v\|^2_{\mathcal{T}_h}, \qquad \|v\|^2_{s_h^3} \lesssim h^{-2-c+\alpha}\|v\|^2_{\mathcal{T}_h}, \tag{7.7}$$

Proof. Since $\|v\|_{a_h^1} \leqslant \|v\|_{a_h^2}$, the proof of (7.6) follows directly from combining the second estimate from (7.4) with the first standard inverse estimate in (7.3). Next, successively applying the last and first inverse estimate recalled in (7.3) shows that for s_h^1 and s_h^2

$$s_h^1(v,v) = h^{1-c}\|[n_F\cdot\nabla v]\|^2_{\mathcal{F}_h} \lesssim h^{-c}\|\nabla v\|^2_{\mathcal{T}_h} = h^{-2}s_h^2(v,v) \lesssim h^{-2-c}\|v\|_{\mathcal{T}_h}. \tag{7.8}$$

Similarly,

$$s_h^3(v,v) = h^{\alpha-c}\|Q_{\Gamma_h}\nabla v\|^2_{\mathcal{T}_h} \lesssim h^{-2-c+\alpha}\|v\|^2_{\mathcal{T}_h}, \tag{7.9}$$

which concludes the proof. □

7.2. **Analysis of the Face-based Stabilization s_h^1.** The analysis of the face-based stabilization was presented in full detail in [4, 6] in the case of codimension $c = 1$. Here, we only note that the proof literally transfers to the general case $c > 1$ after replacing the inverse estimates and fat intersection properties stated in [4, 6] by their properly scaled equivalents introduced in Section 6.4 and Section 7.1. For completeness, we state the final discrete Poincaré estimate.

Lemma 7.4. *For $v \in V_h$ and $0 < h \leq h_0$ with h_0 small enough, it holds*

$$\|v - \lambda_{\Gamma_h}(v)\|^2_{\mathcal{T}_h} \lesssim h^c\|\nabla_{\Gamma_h} v\|^2_{\Gamma_h} + h^{1-c}\|[n_F\cdot\nabla v]\|^2_{\mathcal{F}_h}. \tag{7.10}$$

In particular, for $i = 1, 2$, $\|\cdot\|_{a_h^i} + \|\cdot\|_{s_h^1}$ defines a norm for $v \in V_{h,0}$:

$$h^{-c}\|v\|^2_{\mathcal{T}_h} \lesssim \|v\|^2_{a_h^i} + \|v\|^2_{s_h^1} \quad \text{for } i = 1, 2. \tag{7.11}$$

7.3. **Analysis of the Full Gradient Stabilization s_h^2.** We start with the following lemma which describes how the control of discrete functions on potentially small cut elements can be transferred to their close-by neighbors with large intersections by using the full gradient stabilization term.

Lemma 7.5. *Let $v \in V_h$ and consider two elements $T_1, T_2 \in \mathcal{T}_h$ sharing at least a vertex. Then*

$$\|v\|_{T_1}^2 \lesssim \|v\|_{T_2}^2 + h^2\|\nabla v\|_{T_1}^2, \tag{7.12}$$

with the hidden constant only depending on the quasi-uniformity parameter.

Proof. Let x_0 be a vertex shared by T_1 and T_2 and denote by $v_i = v|_{T_i}$ the restriction of v to T_i. Since v_i is linear,

$$v_i(x) = v_i(x_0) + (x - x_0) \cdot \nabla v_i(x) \tag{7.13}$$

and consequently, using a Young inequality and the fact that the shape regularity implies $|T| \sim h^k$ and $\|x - x_0\|_{L^\infty(T)} \lesssim h$, we see that

$$\|v_1\|_{T_1}^2 \lesssim h^k |v_1(x_0)|^2 + h^2\|\nabla v_1\|_{T_1}^2 \lesssim \|v_2\|_{T_2}^2 + h^2\|\nabla v_1\|_{T_1}^2, \tag{7.14}$$

where we used that $v_1(x_0) = v_2(x_0)$ and an inverse inequality of the form $h^k|v_2(x_0)|^2 \lesssim \|v_2\|_{T_2}^2$. ☐

Now the fat intersection property from Section 6.4 guarantees that Lemma 7.5 only needs to be applied a bounded number of times to transfer the L^2 control from an arbitrary element to an element with a fat intersection. On an element with a fat intersection $h^c|T \cap \Gamma_h| \sim |T|$, the control of the L^2 norm can be passed – via piecewise constant approximations of v – from the element to the discrete manifold part, where $v \in V_h$ satisfies the Poincaré inequality(7.2) on the surface. More precisely, we have the following discrete Poincaré inequality, which involves a scaled version of the L^2 norm of discrete finite element functions on the active mesh.

Lemma 7.6. *For $v \in V_h$, the following estimate holds*

$$h^{-c}\|v - \lambda_{\Gamma_h}(v)\|_{\mathcal{T}_h}^2 \lesssim \|\nabla_{\Gamma_h} v\|_{\Gamma_h}^2 + h^{2-c}\|\nabla v\|_{\mathcal{T}_h}^2 \tag{7.15}$$

for $0 < h \leq h_0$ with h_0 small enough.

Proof. Without loss of generality we can assume that $\lambda_{\Gamma_h}(v) = 0$. After applying (7.12)

$$\|v\|_{\mathcal{T}_h}^2 \lesssim \sum_{x \in \mathcal{X}_h} \|v\|_{\mathcal{T}_{h,x}}^2 \lesssim \sum_{x \in \mathcal{X}_h} \big(\|v\|_{T_x}^2 + h^2\|\nabla v\|_{\mathcal{T}_h}^2\big), \tag{7.16}$$

it is sufficient to proceed with the first term in (7.16). For $v \in V_h$, we define a piecewise constant approximation satisfying $\|v - \overline{v}\|_T \lesssim h\|\nabla v\|_T$, e.g. by taking $\overline{v} = v(x_0)$ for any point $x_0 \in T$. Adding and subtracting $\overline{v}$ gives

$$\sum_{x \in \mathcal{X}_h} \|v\|_{T_x}^2 \lesssim \sum_{x \in \mathcal{X}_h} \|v - \overline{v}\|_{T_x}^2 + \sum_{x \in \mathcal{X}_h} \|\overline{v}\|_{T_x}^2 \tag{7.17}$$

$$\lesssim h^2\|\nabla v\|_{\mathcal{T}_h}^2 + \sum_{x \in \mathcal{X}_h} h^c\|\overline{v}\|_{K_x}^2 \tag{7.18}$$

$$\lesssim h^2\|\nabla v\|_{\mathcal{T}_h}^2 + h^c\|v\|_{\Gamma_h}^2 + \underbrace{h^c\|v - \overline{v}\|_{\Gamma_h}^2}_{\lesssim h^2\|\nabla v\|_{\mathcal{T}_h}^2} \tag{7.19}$$

$$\lesssim h^2\|\nabla v\|_{\mathcal{T}_h}^2 + h^c\|\nabla_{\Gamma_h} v\|_{\Gamma_h}^2, \tag{7.20}$$

where the inverse inequality (7.4) was used in (7.19) to find that $h^c\|v - \overline{v}\|_{K_x}^2 \lesssim \|v - \overline{v}\|_{T_x}^2 \lesssim h^2\|\nabla v\|_{T_x}$, followed by an application of the Poincaré inequality (7.2) in the last step. ☐

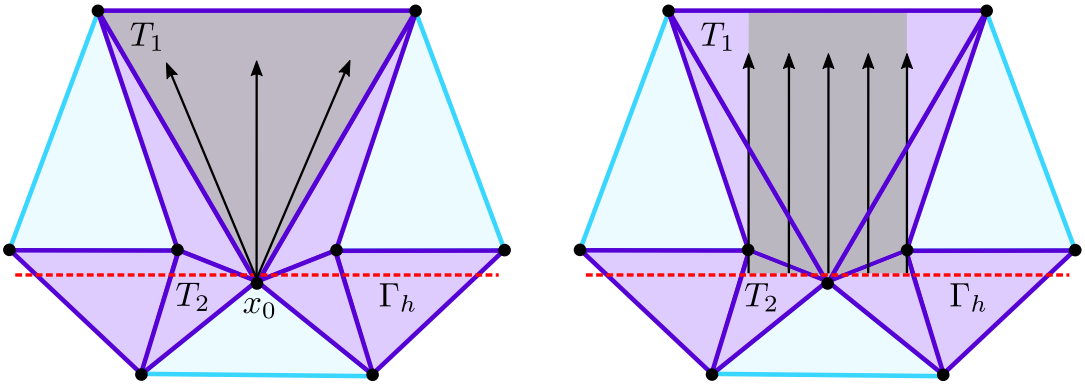

FIGURE 3. Fat intersection properties and L^2 control mechanisms for the full gradient and normal gradient stabilization. (Left) While element T_1 has only a small intersection with Γ_h, there are several neighbor elements in $\mathcal{T}_h$ which share the node x_0 and have a fat intersection with Γ_h. The appearance of the full gradient in stabilization s_h^2 allows to integrate along arbitrary directions and thus gives control of $\|v\|_{T_1}$ through Lemma 7.5. (Right) The fat intersection property for the discrete "normal" tube guarantees that still a significant portion of T_1 can be reached when integrating along normal-like paths which start from Γ_h and which reside completely inside $\mathcal{T}_h$.

7.4. **Analysis of the Normal Gradient Stabilization s_h^3.** The goal of this section is to prove the discrete Poincaré inequality (4.1) by establishing inequality (7.1) for the normal gradient stabilization $s_h^3(v,w) = h^{\alpha-c}(Q_{\Gamma_h}^e \nabla v, Q_{\Gamma_h}^e \nabla w)_{\mathcal{T}_h}$ with $\alpha \in [0,2]$. Recalling the notation from Section 6.5, we start with proving a local variant of (7.2) which involves the normal projection $\overline{Q} = \sum_{i=1}^c \overline{n}_i \otimes \overline{n}_i$ defined by the normal bundle $\{\overline{n}_i\}_{i=1}^c$ associated with the local d-dimensional plane $\overline{\Gamma}$ which approximates Γ_h as specified in Lemma 7.4.

Lemma 7.7. *For $v \in V_h$ and $T \in \mathcal{T}_h$, it holds*

$$\|v\|_T^2 \lesssim h^c \|v\|_{\mathcal{N}(T)\cap\Gamma_h}^2 + h^2 \|\overline{Q}\nabla v\|_{\mathcal{N}(T)}^2, \tag{7.21}$$

where the hidden constant depends only on quasi-uniformity parameter.

Proof. By the fat intersection property (6.59), there is for each $T \in \mathcal{T}_h$ a ball $B_\delta \subset T$ with center x_c and radius $\delta \sim h$ such that $\mathrm{Cyl}(B_\delta, \Gamma_h) \subset \mathcal{N}(T)$. Let $\overline{\Gamma}_2$ be the d-plane parallel with Γ_h and passing through the center x_c. Then taking $\delta' = \sqrt{k}\delta$, the cubular neighborhood $Q_{\delta'} := Q_{\delta'}^c(\overline{\Gamma}_2 \cap B_\delta)$ associated with $\overline{\Gamma}_2$ and its normal bundle $\{\overline{n}_i\}_{i=1}^c$ satisfies $Q_{\delta'} \subset B_\delta$. Since $|Q_{\delta'}| \sim |T|$, a finite dimensionality argument shows that

$$\|v\|_T^2 \lesssim \|v\|_{Q_{\delta'}}^2 \quad \forall\, v \in V_h. \tag{7.22}$$

Next, we apply the scaled Poincaré inequality (6.13) recursively with $\delta' \sim h$ to obtain

$$\begin{aligned}
\|v\|_T^2 &\lesssim \|v\|_{Q_{\delta'}^c}^2 && (7.23)\\
&\lesssim h\|v\|_{Q_{\delta'}^{c-1}}^2 + h^2\|\overline{n}_c \cdot \nabla v\|_{Q_{\delta'}^c}^2 && (7.24)\\
&\lesssim h\big(h\|v\|_{Q_{\delta'}^{c-2}}^2 + h^2\|\overline{n}_{c-1} \cdot \nabla v\|_{Q_{\delta'}^{c-1}}^2\big) + h^2\|\overline{n}_c \cdot \nabla v\|_{Q_{\delta'}^c}^2 && (7.25)\\
&\lesssim h^c\|v\|_{Q_{\delta'}^0}^2 + h^2 \sum_{i=1}^c h^{c-i}\|\overline{n}_i \cdot \nabla v\|_{Q_{\delta'}^i}^2 && (7.26)\\
&\lesssim h^c\|v\|_{\overline{\Gamma}_2\cap B_\delta}^2 + h^2\|\overline{Q}\nabla v\|_T^2, && (7.27)
\end{aligned}$$

where in the last step we used the inverse inequality $\|\overline{n}_i \cdot \nabla v\|_{Q_{\delta'}^i}^2 \lesssim h^{-(c-i)}\|\overline{n}_i \cdot \nabla v\|_T^2$ which can be proven exactly as the inverse inequalities (7.4). It remains to estimate the first term in (7.27).

Recalling the definitions from Section 6.5, we have the representation formula

$$v(x) = v(\overline{p}_h(x)) + \int_0^{\overline{\rho}_h(x)} \overline{n} \cdot \nabla v(\overline{p}_h(x) + s\overline{n}) ds \tag{7.28}$$

for each $x \in \overline{\Gamma}_2 \cap B_\delta$ since $\mathrm{Cyl}(\overline{\Gamma}_2 \cap B_\delta) \subset \mathcal{N}(T)$. Here, $\overline{\rho}_h(x)$ is the distance $\|x - \overline{p}_h(x)\|_{\mathbb{R}^k}$ satisfying $\overline{\rho}_h(x) \sim h$, and $\overline{n}$ is the unit normal vector corresponding to $x - \overline{p}_h(x)$. As before, we deduce that

$$|v(x)|^2 \lesssim |v(\overline{p}_h(x)|^2 + h \int_0^{\overline{\rho}_h(x)} |\overline{n} \cdot \nabla v(\overline{p}_h(x) + s\overline{n})|^2 ds. \tag{7.29}$$

After integrating over $\overline{\Gamma}_2 \cap B_\delta$ we get

$$\int_{\overline{\Gamma}_2 \cap B_\delta} v^2 \, \mathrm{d}\overline{\Gamma}_2(x) \lesssim \int_{\overline{\Gamma}_2 \cap B_\delta} (v \circ \overline{p}_h(x))^2 \, \mathrm{d}\overline{\Gamma}_2(x) + h \int_{\overline{\Gamma}_2 \cap B_\delta} \int_0^{\overline{\rho}_h(x)} |\overline{n} \cdot \nabla v(\overline{p}_h(x) + s\overline{n})|^2 ds \, \mathrm{d}\overline{\Gamma}_2(x) \tag{7.30}$$

$$\lesssim \int_{\Gamma_h \cap \mathcal{N}(T)} v(x)^2 \, \mathrm{d}\Gamma_h(x) + h \int_{\Gamma_h \cap \mathcal{N}(T)} \int_0^{\overline{\rho}_h(x)} |\overline{n} \cdot \nabla v(x + s\overline{n})|^2 ds \, \mathrm{d}\Gamma_h(x). \tag{7.31}$$

Observe that the last term in (7.31) is the integral of the discrete function $|\overline{n} \cdot \nabla v(x + s\overline{n})|^2$ over a $(c-1)$-codimensional subset of $\mathrm{Cyl}(\overline{\Gamma}_2 \cap B_\delta) \subset \mathcal{N}(T)$, and thus an inverse inequality similar to (7.4) gives

$$h \int_{\Gamma_h \cap \mathcal{N}(T)} \int_0^{\overline{\rho}_h(x)} |\overline{n} \cdot \nabla v(x + s\overline{n})|^2 ds \, \mathrm{d}\Gamma_h(x) \lesssim h \cdot h^{-c+1} \|\overline{n} \cdot \nabla v\|^2_{\mathcal{N}(T)}, \tag{7.32}$$

and therefore

$$\|v\|^2_{\overline{\Gamma}_2 \cap B_\delta} \lesssim \|v\|^2_{\Gamma_h \cap \mathcal{N}(T)} + h^{2-c} \|\overline{Q} \nabla v\|^2_{\mathcal{N}(T)}. \tag{7.33}$$

Now inserting (7.33) into (7.27) concludes the proof. □

Thanks to the geometric approximation properties (6.55), the previous lemma gives us the leverage to prove the main result of this section.

Proposition 7.8. *Assume that $v \in V_h$. Then*

$$h^{-c} \|v\|^2_{\mathcal{T}_h} \lesssim \|v\|^2_{\Gamma_h} + s_h^3(v, v), \tag{7.34}$$

$$h^{-c} \|v - \lambda_{\Gamma_h}(v)\|^2_{\mathcal{T}_h} \lesssim \|\nabla_{\Gamma_h} v\|^2_{\Gamma_h} + s_h^3(v, v). \tag{7.35}$$

Proof.

$$\|v\|^2_{\mathcal{T}_h} = \sum_{T \in \mathcal{T}_h} \|v\|^2_T \lesssim \sum_{T \in \mathcal{T}_h} \left(h^c \|v\|^2_{\mathcal{N}(T) \cap \Gamma_h} + h^2 \|\overline{Q} \nabla v\|^2_{\mathcal{N}(T)} \right) \tag{7.36}$$

$$\lesssim h^c \|v\|^2_{\Gamma_h} + \sum_{T \in \mathcal{T}_h} h^2 \left(\|Q_{\Gamma_h} \nabla v\|^2_{\mathcal{N}(T)} + \|(Q^e_{\Gamma_h} - \overline{Q}) \nabla v\|^2_{\mathcal{N}(T)} \right) \tag{7.37}$$

$$\lesssim h^c \|v\|^2_{\Gamma_h} + h^2 \|Q^e_{\Gamma_h} \nabla v\|^2_{\mathcal{T}_h} + h^4 \|\nabla v\|^2_{\mathcal{T}_h} \tag{7.38}$$

$$\lesssim h^c \|v\|^2_{\Gamma_h} + h^2 \|Q^e_{\Gamma_h} \nabla v\|^2_{\mathcal{T}_h} + h^2 \|v\|^2_{\mathcal{T}_h}. \tag{7.39}$$

For h small enough, the last term in (7.39) can be kick-backed to the left-hand side and as a result

$$h^{-c} \|v\|^2_{\mathcal{T}_h} \lesssim \|v\|_{\Gamma_h} + h^{2-c} \|Q^e_{\Gamma_h} \nabla v\|^2_{\mathcal{T}_h} \lesssim \|v\|^2_{\Gamma_h} + s_h^3(v, v). \tag{7.40}$$

The Poincaré inequality (7.35) then follows directly from combining (7.34) and (7.2). □

Remark 7.9. In the previous proof, the kick-back argument used to pass from $\overline{Q}$ to the actual discrete normal projection Q_{Γ_h} used only the fact that $\|\overline{Q} - Q_{\Gamma_h}\|_{L^\infty(\mathcal{N}(T))} = o(1)$ for $h \to 0$. Consequently, Proposition 7.8 remains valid when Γ_h and $\{n_i^h\}_{i=1}^c$ satisfy higher order approximation assumptions of the form $\|\rho\|_{L^\infty(\Gamma_h)} + h\|Q^e_\Gamma - Q_{\Gamma_h}\|_{L^\infty(\Gamma_h)} \lesssim h^k$ for $k > 1$.

8. An Interpolation Operator: Construction and Estimates

The main goal of this section is to construct a suitable interpolation operator and to show that it satisfies the approximation assumption (5.14). We start with the following lemma.

Lemma 8.1. *The extension operator v^e defines a bounded operator $H^m(\Gamma) \ni v \mapsto v^e \in H^m(U_\delta(\Gamma))$ satisfying the stability estimate*

$$\|v^e\|_{l,U_\delta(\Gamma)} \lesssim \delta^{c/2}\|v\|_{l,\Gamma}, \qquad 0 \leqslant l \leqslant m, \tag{8.1}$$

for $0 < \delta \leqslant \delta_0$, where the hidden constant depends only on the curvature of Γ.

Proof. Again, by a partition of unity argument, we can assume that Γ is given by a single parametrization. Recalling the definition of v^e and using tube coordinates (6.4) defined by Φ in combination with the measure equivalence (6.8), the tube integral for $l = 0$ computes to

$$\|v^e\|^2_{0,U_\delta(\Gamma)} = \int_{\widetilde{W}} \left(\int_{B^c_\delta(0)} |u^e(y,s)|^2 \sqrt{g^\Phi(y,s)}\, \mathrm{d}s \right) \mathrm{d}y \tag{8.2}$$

$$\sim \int_{\widetilde{W}} \left(\int_{B^c_\delta(0)} |u^e(y,0)|^2 \, \mathrm{d}s \right) \sqrt{g^\alpha(y)}\, \mathrm{d}y \tag{8.3}$$

$$\sim \delta^c \int_\Gamma |u|^2 \, \mathrm{d}\Gamma. \tag{8.4}$$

For $l > 0$, simply combine a similar integral computation with a successive application of the identity $Dv^e = Dv \circ Dp$ and the boundedness of $D^l p$. □

Next, we recall from [16] that for $v \in H^m(\mathcal{T}_h)$, the standard Clément interpolant $\pi_h : L^2(N_h) \to V_h$ satisfies the local interpolation estimates

$$\|v - \pi_h v\|_{l,T} \lesssim h^{m-l}|v|_{m,\omega(T)}, \qquad 0 \leqslant l \leqslant m \qquad \forall\, T \in \mathcal{T}_h, \tag{8.5}$$

$$\|v - \pi_h v\|_{l,F} \lesssim h^{m-l-1/2}|v|_{m,\omega(F)}, \quad 0 \leqslant l \leqslant m - 1/2 \quad \forall\, F \in \mathcal{F}_h, \tag{8.6}$$

where $\omega(T)$ consists of all elements sharing a vertex with T and the patch $\omega(F)$ is defined analogously. With the help of the extension operator, we construct an interpolation operator via

$$H^m(\Gamma) \ni v \mapsto \pi_h v^e \in V_h, \tag{8.7}$$

where we used the fact that $N_h = \cup_{T\in\mathcal{T}_h} T \subset U_{\delta_0}(\Gamma)$ for $h \lesssim \delta_0$. Before we state and prove the main interpolation result, we consider the interpolation error in the semi-norm $\|\cdot\|_{s_h}$ induced by the stabilization form s_h.

Lemma 8.2. *For $v \in H^2(\Gamma)$ and any stabilization form s_h from Table 1, it holds that*

$$\|v^e - \pi_h v^e\|_{s_h} \lesssim h\|v\|_{2,\Gamma}. \tag{8.8}$$

Proof. For the face-based stabilization s^1_h, the desired estimate follows directly from the interpolation estimate (8.6), the bounded number of patch overlaps $\omega(F)$ and the stability result (8.1)

$$\|v^e - \pi_h v^e\|^2_{s^1_h} = h^{1-c}\|n_F \cdot [\nabla(v^e - \pi_h v^e)]\|^2_{\mathcal{F}_h} \tag{8.9}$$

$$\lesssim h^{1-c} \sum_{F\in\mathcal{F}_h} h\|v^e\|^2_{2,\omega(F)} \lesssim h^{2-c}\|v^e\|^2_{2,U_\delta(\Gamma)} \lesssim h^2\|v\|^2_{2,\Gamma}, \tag{8.10}$$

where $\delta \sim h$. Similarly, we see that for the full gradient and normal gradient stabilization it holds

$$\|v^e - \pi_h v^e\|^2_{s^2_h} = h^{2-c}\|\nabla(v^e - \pi_h v^e)\|^2_{\mathcal{T}_h} \lesssim h^4\|v\|^2_{2,\Gamma}, \tag{8.11}$$

$$\|v^e - \pi_h v^e\|^2_{s^3_h} = h^{\alpha-c}\|Q^e_{\Gamma_h}\nabla(v^e - \pi_h v^e)\|^2_{\mathcal{T}_h} \lesssim h^{2+\alpha}\|v\|^2_{2,\Gamma}, \tag{8.12}$$

which in the normal gradient case gives the desired approximation order for $\alpha \geqslant 0$. □

To prepare the proof of the desired interpolation properties for the interpolant $\pi_h v^e$, we recall that the standard scaled trace inequality

$$\|v\|_{\partial T} \lesssim h^{-\frac{1}{2}}\|v\|_T + h^{\frac{1}{2}}\|\nabla v\|_T \tag{8.13}$$

is valid for $v \in H^1(T)$ and $T \in \mathcal{T}_h$. Previous proofs [4, 31] of interpolation properties for the interpolant $\pi_h v^e$ used a similar scaled trace inequality of the form

$$\|v^e\|_{\Gamma_h} \lesssim h^{-\frac{1}{2}}\|v^e\|_{\mathcal{T}_h} + h^{\frac{1}{2}}\|\nabla v^e\|_{\mathcal{T}_h} \tag{8.14}$$

in the case where Γ_h is a Lipschitz surface of codimension $c = 1$. We point out that the standard proof to establish such a scaled trace inequality relies on a combination of the divergence theorem and the fact that Γ_h splits the element T into two subdomains, see [20, 22]. Consequently, the proof is not applicable in the case of codimension $c > 1$. Here, we present a proof which is valid for any codimension. The idea is roughly to successively "climb up" from Γ to the full tubular neighborhood $U_\delta(\Gamma)$ via the i-th cubular neighborhoods Q^i_δ by using the trace inequality from Lemma 6.1.

Theorem 8.3. *For $v \in H^2(\Gamma)$, it holds that*

$$\|v^e - \pi_h v^e\|_{\Gamma_h} + h\|v^e - \pi_h v^e\|_{A_h} \lesssim h^2\|v\|_{2,\Gamma}. \tag{8.15}$$

Proof. By definition, $\|\cdot\|^2_{A_h} = \|\cdot\|^2_{a_h} + \|\cdot\|^2_{s_h}$ and thanks to Lemma 8.2 and the choices of a_h given in Section 3.3, it is sufficient to prove that

$$\|v^e - \pi_h v^e\|_{\Gamma_h} + h\|D(v^e - \pi_h v^e)\|_{\Gamma_h} \lesssim h^2\|v\|_{2,\Gamma}. \tag{8.16}$$

Clearly, Γ can be covered by local coordinate neighborhoods satisfying the assumptions of Lemma 6.1. The quasi-uniformity of $\mathcal{T}_h$ and the fact that $\operatorname{dist}(\Gamma, T) \lesssim h$ implies that there is a simplex $\widetilde{T}$ similar to T with $\operatorname{diam}(\widetilde{T}) \sim h$ such that the chain of inclusions $T \subset Q^c_\delta(p(T)) \subset \widetilde{T}$ holds with $\delta \sim h$. Sometimes we also write $\widetilde{T}(T)$ if we want to emphasize that the considered $\widetilde{T}$ is picked for a particular T. Consequently, there is a $\widetilde{v}_T \in P_1(\widetilde{T})$ satisfying the interpolation estimate

$$\|v^e - \widetilde{v}_T\|_{\widetilde{T}} + h\|D(v^e - \widetilde{v}_T)\|_{\widetilde{T}} \lesssim h^2\|v^e\|_{H^2(\widetilde{T})}. \tag{8.17}$$

Restricting $\widetilde{v}_T$ to Γ and denoting its subsequent extension $(\widetilde{v}_T|_\Gamma)^e$ simply by $\widetilde{v}^e_T$, we obtain

$$\begin{aligned}\|v^e - \pi_h v^e\|^2_{\Gamma_h} + h^2\|D(v^e - \pi_h v^e)\|^2_{\Gamma_h} \lesssim{}& \sum_{T\in\mathcal{T}_h}\Big(\|v^e - \widetilde{v}^e_T\|^2_{T\cap\Gamma_h} + h^2\|D(v^e - \widetilde{v}^e_T)\|^2_{T\cap\Gamma_h}\Big)\\ &+ \sum_{T\in\mathcal{T}_h}\Big(\|\widetilde{v}^e_T - \pi_h v^e\|^2_{T\cap\Gamma_h} + h^2\|D(\widetilde{v}^e_T - \pi_h v^e)\|^2_{T\cap\Gamma_h}\Big) \qquad (8.18)\\ ={}& I + II, \qquad (8.19)\end{aligned}$$

which we estimate next.

Term *I*. We start with lifting each discrete manifold part $\Gamma_h \cap T$ to Γ which gives

$$\begin{aligned} I &\lesssim \sum_{T\in\mathcal{T}_h}\|v - \widetilde{v}_T\|^2_{(T\cap\Gamma_h)^l} + h^2\|D(v - \widetilde{v}_T)\|^2_{(T\cap\Gamma_h)^l} &(8.20)\\ &\lesssim \sum_{T\in\mathcal{T}_h}\|v - \widetilde{v}_T\|^2_{p(T)} + h^2\|D(v - \widetilde{v}_T)\|^2_{p(T)}. &(8.21)\end{aligned}$$

Then apply the scaled trace estimate (6.12) on each projected element $Q^0_\delta(p(T)) = p(T) \subset \Gamma$ to see that

$$\begin{aligned}\|v - \widetilde{v}_T\|^2_{Q^0_\delta(p(T))} + h^2\|D(v - \widetilde{v}_T)\|^2_{Q^0_\delta(p(T))} \lesssim h^{-1}\Big(&\|v^e - \widetilde{v}_T\|^2_{Q^1_\delta(p(T))} + h^2\|D(v^e - \widetilde{v}_T)\|^2_{Q^1_\delta(p(T))}\\ &+ h^4\|D^2 v^e\|_{Q^1_\delta(p(T))}\Big). \qquad (8.22)\end{aligned}$$

After reiterating the argument and applying (6.12) to $\|\cdot\|_{Q^i_\delta(p(T))}$ for $i = 1, \dots, c$, we arrive at

$$\|v - \widetilde{v}_T\|^2_{Q^0_\delta(p(T))} + h^2\|D(v - \widetilde{v}_T)\|^2_{Q^0_\delta(p(T))} \lesssim h^{-c}\Big(\|v^e - \widetilde{v}_T\|^2_{Q^c_\delta(p(T))} + h^2\|D(v^e - \widetilde{v}_h)\|^2_{Q^c_\delta(p(T))}\Big) + \sum_{i=1}^{c} h^{4-i}\|D^2 v^e\|^2_{Q^i_\delta(p(T))} \tag{8.23}$$

$$= I_a + I_b. \tag{8.24}$$

Recalling that $Q^c_\delta(p(T)) \subset \widetilde{T}$ and that $\widetilde{v}_T$ satisfies (8.17), the term I_a can be further estimated,

$$\sum_{T\in\mathcal{T}_h} I_a \lesssim h^{-c}h^4\|D^2 v^e\|^2_{\widetilde{T}(T)} \lesssim h^{-c}h^4\|D^2 v^e\|^2_{Q^c_\delta(\Gamma)} \lesssim h^4\|v\|^2_{2,\Gamma}, \tag{8.25}$$

where we used the stability estimate (8.1) and the fact that number of overlaps between similar simplices $\widetilde{T}(T)$ and $\widetilde{T}(T')$ is uniformly bounded in T; that is,

$$\#\{T' \in \mathcal{T}_h : \widetilde{T}(T) \cap \widetilde{T}(T') \neq \emptyset\} \lesssim 1 \quad \forall\, T \in \mathcal{T}_h. \tag{8.26}$$

Similarly, each projected element $p(T)$ is only overlapped by a uniformly bounded number of other projected elements $p(T')$ and therefore the remaining term I_b can be bounded by

$$\sum_{T\in\mathcal{T}_h} I_b \lesssim \sum_{i=1}^{c}\sum_{T\in\mathcal{T}_h} h^4\|D^2 v\|_{p(T)} \lesssim h^4\|D^2 v\|_\Gamma, \tag{8.27}$$

where in the first step, a stability estimate of the form (8.1) with $U_\delta(\Gamma)$ replaced by $Q^i_\delta(\Gamma)$ was used for $i = 1, \dots, c$ and $\delta \sim h$.

Term II. A successive application of the inverse inequalities (7.4), (7.3) and a triangle inequality yields to

$$II \lesssim h^{-c}\|\widetilde{v}^e_T - \pi_h v^e\|^2_{\mathcal{T}_h} \lesssim h^{-c}\|v^e - \pi_h v^e\|^2_{\mathcal{T}_h} + h^{-c}\|v^e - \widetilde{v}^e_T\|^2_{\mathcal{T}_h} = II_a + II_b. \tag{8.28}$$

With the interpolation estimate (8.5) and stability bound (8.1), term II_a can be estimated by

$$II_a \lesssim h^{-c}h^4\|D^2 v^e\|^2_{\mathcal{T}_h} \lesssim h^4\|v\|^2_{2,\Gamma}. \tag{8.29}$$

Referring to (8.21) , the remaining term II_b can be treated exactly as Term I by observing that

$$II_b \lesssim \sum_{T\in\mathcal{T}_h} h^{-c}\|v^e - \widetilde{v}^e_T\|^2_{U^c_h(p(T))} \lesssim \sum_{T\in\mathcal{T}} \|v^e - \widetilde{v}^e_T\|^2_{p(T)} \lesssim h^4\|v\|^2_{2,\Gamma}. \tag{8.30}$$

where again the interpolation property (8.17) and the final overlap property (8.26) was used. This concludes the proof. □

9. Verification of the Quadrature and Consistency Error Estimates

Finally, with the help of the geometric estimate established in Section 6, we now show that for the proposed cut finite element realizations the quadrature and consistency error satisfy assumption (5.15)–(5.18) and (5.19).

Lemma 9.1. *Let the discrete linear form l_h be defined by (3.22) and assume that the discrete bilinear form a_h is given by either a^1_h or a^2_h from Table 1. Then*

$$|l_h(v) - l(v^l)| \lesssim h^2\|f\|_\Gamma\|v\|_{A_h} \quad \forall\, v \in V_{0,h}, \tag{9.1}$$

$$|a(u, v^l) - a_h(u^e, v)| \lesssim h\|u\|_{2,\Gamma}\|v\|_{A_h} \quad \forall\, u \in H^2(\Gamma) \cap H^1(\Gamma)/\mathbb{R},\ \forall\, v \in V_h. \tag{9.2}$$

Furthermore, for $\phi \in H^2(\Gamma)$ and $\phi_h = \pi_h\phi$ the following improved estimates hold

$$|l_h(\phi_h) - l(\phi^l_h)| \lesssim h^2\|f\|_\Gamma\|\phi\|_{2,\Gamma}, \tag{9.3}$$

$$|a(u^l_h, \phi^l_h) - a_h(u_h, \phi_h)| \lesssim h^2\|u\|_{2,\Gamma}\|\phi\|_{2,\Gamma}. \tag{9.4}$$

Proof. We start with proving (9.1). For the quadrature error of l_h side we have

$$l(v^l) - l_h(v) = (f, v^l)_\Gamma - (f^e, v)_{\Gamma_h} = (f, v^l(1 - |B|_d^{-1}))_\Gamma \lesssim h^2 \|f\|_\Gamma \|v^l\|_\Gamma \lesssim h^2 \|f\|_\Gamma \|v\|_{A_h}, \quad (9.5)$$

where in the last step, the Poincaré inequality (7.2) was used after passing from Γ to Γ_h. Since the interpolation estimate (5.14) yields the simple bound $\|\pi_h \phi\|_{A_h} \lesssim \|\phi\|_{2,\Gamma}$, estimate (9.3) follows immediately.

Turning to estimate (9.2) and (9.4) and applying the splitting $\nabla = \nabla_{\Gamma_h} + Q_{\Gamma_h}\nabla$ we see that

$$a_h^2(u^e, v) = (\nabla_{\Gamma_h} u^e, \nabla_{\Gamma_h} v)_{\Gamma_h} + (Q_{\Gamma_h}\nabla u^e, Q_{\Gamma_h}\nabla v)_{\Gamma_h} = a_h^1(u^e, v) + (Q_{\Gamma_h}\nabla u^e, Q_{\Gamma_h}\nabla v)_{\Gamma_h}, \quad (9.6)$$

and thus it is enough to consider only the case $a_h = a_h^2$. Using this decomposition we obtain

$$\begin{aligned} a(u, v^l) - a_h(u^e, v) &= \big((\nabla_\Gamma u, \nabla_\Gamma v^l)_\Gamma - (\nabla_{\Gamma_h} u^e, \nabla_{\Gamma_h} v)_{\Gamma_h}\big) - (Q_{\Gamma_h}\nabla u^e, Q_{\Gamma_h}\nabla v)_{\Gamma_h} && (9.7)\\ &= I + II. && (9.8)\end{aligned}$$

A bound for the first term I can be derived by lifting the tangential part of $a_h(\cdot,\cdot)$ to Γ and employing the bounds for determinant (6.43), the operator norm estimates (6.35), and the norm equivalences (6.49)–(6.50),

$$\begin{aligned} I &= (\nabla_\Gamma u, \nabla_\Gamma v^l)_\Gamma - (\nabla_{\Gamma_h} u^e, \nabla_{\Gamma_h} v)_{\Gamma_h} && (9.9)\\ &= (\nabla_\Gamma u, \nabla_\Gamma v^l)_\Gamma - ((\nabla_{\Gamma_h} u^e)^l, (\nabla_{\Gamma_h} v)^l |B|^{-1})_\Gamma && (9.10)\\ &= \big((P_\Gamma - |B|^{-1} BB^T)\nabla_\Gamma u, \nabla_\Gamma v^l\big)_\Gamma && (9.11)\\ &= \big((P_\Gamma - BB^T) + (1 - |B|^{-1})BB^T)\nabla_\Gamma u, \nabla_\Gamma v^l\big)_\Gamma && (9.12)\\ &\lesssim h^2 \|\nabla_\Gamma u\|_\Gamma \|\nabla_\Gamma v^l\|_\Gamma && (9.13)\\ &\lesssim h^2 \|f\|_\Gamma \|\nabla_\Gamma v^l\|_\Gamma, && (9.14)\end{aligned}$$

In the last step, we used the simple stability estimate $\|\nabla_\Gamma u\|_\Gamma \lesssim \|f\|_\Gamma$ which is an immediate consequence of the weak formulation (2.12). Again, for $\phi_h = \pi_h \phi$, the improved estimate (9.4) follows from $\|\nabla_\Gamma \phi_h^l\|_\Gamma \lesssim \|\phi_h\|_{A_h} \lesssim \|\phi\|_{2,\Gamma}$. Turning to the second term II and applying the inequality (6.37) to $Q_{\Gamma_h}\nabla u^e$ gives

$$\begin{aligned} II &\lesssim \|Q_{\Gamma_h}\nabla u^e\|_{\Gamma_h} \|Q_{\Gamma_h}\nabla v\|_{\Gamma_h} && (9.15)\\ &\lesssim h \|f\|_\Gamma \|Q_{\Gamma_h}\nabla v\|_{\Gamma_h}. && (9.16)\end{aligned}$$

For general $v \in V_h$, the last factor in II is simply bounded by $\|\nabla v\|_{\Gamma_h}$ while in the special case $v = \pi_h \phi^e$, the interpolation estimate (8.15) and a second application of (6.37) to $Q_{\Gamma_h}\nabla \phi^e$ yields

$$\|Q_{\Gamma_h}\nabla \pi_h \phi^e\|_{\Gamma_h} \lesssim \|Q_{\Gamma_h}\nabla \phi^e\|_{\Gamma_h} + \|Q_{\Gamma_h}\nabla(\phi^e - \pi_h \phi^e)\|_{\Gamma_h} \lesssim h\|\phi\|_{2,\Gamma}. \quad (9.17)$$

□

We conclude this section by commenting on the consistency of the proposed cut finite element formulations. First note that $s_h^1(u^e, u^e) = 0$ for $u \in H^2(\Gamma)$ since $u^e \in H^2(U_\delta(\Gamma))$. On the other hand, the stability estimate (8.1) with $\delta \sim h$ shows that $h^{2-c}\|\nabla u^e\|_{\mathcal{T}_h}^2 \lesssim h^2 \|u\|_{2,\Gamma}^2$ and thus the weak consistency assumption (5.19) holds for s_h^2. Finally, for the normal gradient s_h^3 we see that thanks to (3.5),

$$h^{\alpha-c}\|Q_{\Gamma_h}\nabla u^e\|_{\mathcal{T}_h}^2 = h^{\alpha-c}\|(Q_{\Gamma_h} - Q_\Gamma^e)\nabla u^e\|_{\mathcal{T}_h}^2 \lesssim h^{\alpha-c+2}\|\nabla u^e\|_{\mathcal{T}_h}^2 \lesssim h^{\alpha+2}\|\nabla_\Gamma u\|_\Gamma^2, \quad (9.18)$$

and thus any choice $\alpha \in [0, 2]$ ensures a weakly consistent stabilization which satisfies the Poincaré inequality (4.1).

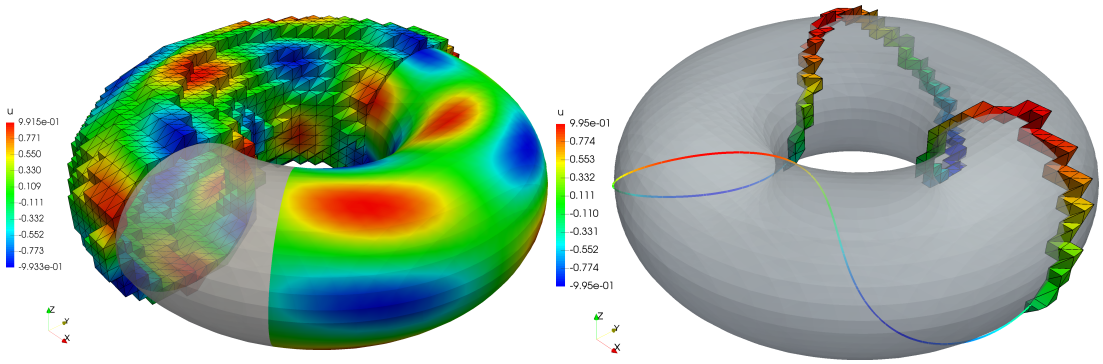

FIGURE 4. Solution plots. Each plot shows the numerical solution u_h computed on the active mesh $\mathcal{T}_h$ and its restriction to the manifold discretization $\mathcal{K}_h$. (Left) Solution for the surface example computed on $\mathcal{T}_2$ with $h \approx 0.22 \cdot 10^{-2}$ using the normal gradient stabilized tangential form $a_h^1 + s_h^3$ with $\tau = 1.0$. (Right) Solution for curve example on $\mathcal{T}_2$ with same mesh size using the full gradient stabilized full gradient form $a_h^2 + s_h^2$ with $\tau = 1.0$.

10. Numerical Results

In this final section we complement the development of the theoretical framework with a number of numerical studies which validate the theoretically proven bounds on condition number and the a priori error as stated in Theorem 5.4 and 4.2, respectively. With $\mathbb{R}^3$ as embedding space, we consider examples for codimension 1 and 2. The main goal of the presented examples is to corroborate the theoretical findings, but more in-depth numerical studies comparing the properties of some of the presented stabilization terms can be found in [7] for the codim = 1 case.

10.1. **Convergence Rates for the Laplace-Beltrami Problem on a Torus.** In the first convergence rate study, we define total bilinear form A_h by combining the full gradient form a_h^2 with the normal gradient stabilization s_h^3,

$$A_h(u_h, v_h) = (\nabla u_h, \nabla v_h)_{\mathcal{K}_h} + \tau h (n_{\Gamma_h} \cdot \nabla u_h, n_{\Gamma_h} \cdot \nabla v_h)_{\mathcal{T}_h} \tag{10.1}$$

with $\tau = 0.1$ to discretize the Laplace-Beltrami type problem

$$-\Delta_\Gamma u + u = f \quad \text{on } \Gamma \tag{10.2}$$

on the torus surface Γ defined by

$$\Gamma = \{x \in \mathbb{R}^3 : r^2 = x_3^2 + (\sqrt{x_1^2 + x_2^2} - R)^2\}, \tag{10.3}$$

with major radius $R = 1.0$ and minor radius $r = 0.5$. Based on the parametrization

$$x = \gamma(\phi, \theta) = R \begin{pmatrix} \cos\phi \\ \sin\phi \\ 0 \end{pmatrix} + r \begin{pmatrix} \cos\phi\cos\theta \\ \sin\phi\cos\theta \\ \sin\theta \end{pmatrix}, \quad (\phi, \theta) \in [0, 2\pi) \times [0, 2\pi), \tag{10.4}$$

an analytical reference solution u with corresponding right-hand side f is given by

$$u(x) = \sin(3\phi)\cos(3\theta + \phi), \tag{10.5}$$

$$\begin{aligned} f(x) = {} & r^{-2}(9\sin(3\phi)\cos(3\theta+\phi) \\ & + (R + r\cos(\theta))^{-2}(10\sin(3\phi)\cos(3\theta+\phi) + 6\cos(3\phi)\sin(3\theta+\phi)) \\ & + (r(R + r\cos(\theta)))^{-1}(3\sin(\theta)\sin(3\phi)\sin(3\theta+\phi)) + u(x(\phi,\theta)). \end{aligned} \tag{10.6}$$

To examine the convergence rates predicted by Theorem 5.4, we generate a sequence of meshes $\{\mathcal{T}_k\}_{k=0}^5$ by uniformly refining an initial structured background mesh $\widetilde{\mathcal{T}}_0$ for $\Omega = [-1.1, 1.1]^3 \supset \Gamma$ with mesh size $h = 0.22$. At each refinement level k, the mesh $\mathcal{T}_k$ is then given by the active

(background) mesh as defined in (3.7). For a given error norm, the corresponding experimental order of convergence (EOC) at refinement level k is calculated using the formula

$$\mathrm{EOC}(k) = \frac{\log(E_{k-1}/E_k)}{\log(2)},$$

with E_k denoting the error of the computed solution u_k at refinement level k. The resulting errors for the $\|\cdot\|_{H^1(\Gamma_h)}$ and $\|\cdot\|_{L^2(\Gamma_h)}$ norms are summarized in Table 2 (left) and confirm the first-order and second-order convergences rates predicted by Theorem 5.4. Finally, the discrete solution computed at refinement level $k = 2$ is visualized in Figure 4 (left).

10.2. **Convergence Rates for the Laplace-Beltrami Problem on a Torus Line.** Next, we solve problem (10.2) on the 1-dimensional manifold $\Gamma \subset \mathbb{R}^3$ defined by the torus line

$$x = \gamma(t, Nt) = R\begin{pmatrix}\cos(t)\\ \sin(t)\\ 0\end{pmatrix} + r\begin{pmatrix}\cos(t)\cos(Nt)\\ \sin(t)\cos(Nt)\\ \sin(Nt)\end{pmatrix}, \quad t \in [0, 2\pi), \tag{10.7}$$

where N determines "the winding number" of the curve γ with respect to the torus centerline $\{x \in \mathbb{R}^3 : x_1^2 + x_2^2 = R^2 \wedge x_3 = 0\}$. We set $R = 2r = 1.0$ and $N = 3$. This time, the full gradient form a_h^2 augmented by the full gradient stabilization s_h^2 constitutes the overall bilinear form

$$A_h(u_h, v_h) = (\nabla u_h, \nabla v_h)_{\mathcal{K}_h} + \tau(\nabla u_h, \nabla v_h)_{\mathcal{T}_h} \tag{10.8}$$

to compute the discrete solution u_h. To examine the convergence properties of the scheme, we consider the manufactured solution given by

$$u(x) = \sin(3t), \tag{10.9}$$

$$f(x) = 36\frac{-64\sin^5(t) - 128\sin^4(t)\sin(3t) + 2\sin(3t)\cos(3t) + 41\sin(3t) - 28\sin(5t) + 8\sin(7t)}{\left(128\sin^6(t) - 192\sin^4(t) + 72\sin^2(t) - 9\sin^2(3t) + 4\cos(3t) + 14\right)^2}. \tag{10.10}$$

Similar to the previous example, we generate a series of successively refined active background meshes $\{\mathcal{T}_k\}_{k=0}^5$ with $h_k = 0.22/N_k$ and $N_k = 10 \cdot 2^k$. To define a suitable discretization of Γ, we first subdivide the parameter interval $[0, 2\pi)$ into $10 \cdot N_k$ subintervals of equal length. The collection of segments connecting the mapped endpoints of each subinterval to Γ defines an initial partition $\widetilde{\mathcal{K}}_k$ of the curve γ. Then a compatible partition $\mathcal{K}_k$ is generated by computing all non-trivial intersections $K \cap T$ for $K \in \widetilde{\mathcal{K}}_k$, $T \in \mathcal{T}_k$ and partitioning each segment K accordingly. A plot of the computed solution at refinement level $k = 2$ is shown in Figure 4 (right). As before, the observed reduction of the $\|\cdot\|_{H^1(\Gamma_h)}$ and $\|\cdot\|_{L^2(\Gamma_h)}$ discretization error confirms the predicted convergences rates, see Table 2 (right).

k	$\|u_k - u\|_{1,\Gamma_h}$	EOC	$\|u_k - u\|_{\Gamma_h}$	EOC
0	$9.99{\cdot}10^{0}$	–	$1.16{\cdot}10^{0}$	–
1	$5.54{\cdot}10^{0}$	0.85	$4.33{\cdot}10^{-1}$	1.43
2	$2.80{\cdot}10^{0}$	0.98	$1.18{\cdot}10^{-1}$	1.87
3	$1.42{\cdot}10^{0}$	0.98	$3.05{\cdot}10^{-2}$	1.95
4	$7.14{\cdot}10^{-1}$	0.99	$7.74{\cdot}10^{-3}$	1.98
5	$3.58{\cdot}10^{-1}$	1.00	$1.95{\cdot}10^{-3}$	1.99

k	$\|u_k - u\|_{1,\Gamma_h}$	EOC	$\|u_k - u\|_{\Gamma_h}$	EOC
0	$1.77{\cdot}10^{0}$	–	$8.59{\cdot}10^{-1}$	–
1	$7.48{\cdot}10^{-1}$	1.24	$2.74{\cdot}10^{-1}$	1.65
2	$3.75{\cdot}10^{-1}$	1.00	$6.66{\cdot}10^{-2}$	2.04
3	$1.91{\cdot}10^{-1}$	0.98	$1.71{\cdot}10^{-2}$	1.96
4	$9.77{\cdot}10^{-2}$	0.96	$4.36{\cdot}10^{-3}$	1.97
5	$4.79{\cdot}10^{-2}$	1.03	$1.09{\cdot}10^{-3}$	2.01

TABLE 2. Convergence rates for the surface example (left) and curve example (right).

10.3. **Condition Number Tests.** The final section is devoted to the numerical study of the dependency of the condition number on the mesh size and on the positioning of the embedded manifold in the background mesh. Again, we consider the case of a surface and a curve embedded into $\mathbb{R}^3$ and pick the unit-sphere $S^2 = \{x \in \mathbb{R}^3 : \|x\| = 1\}$ and the torus line defined by (10.7) as example manifolds of codimension 1 and 2, respectively. For each case, we choose the same bilinear form A_h as in the corresponding convergence rate test.

For each considered manifold Γ, we generate a sequence $\{\mathcal{T}_k\}_{k=0}^5$ of tessellations of $\Omega = [-1.6, 1.6]^3$ with mesh size $h = 3.2/k$ for $k \in \{10, 15, 20, 30, 40, 60\}$. To study the influence of the relative position on the condition number, we generate for each mesh $\mathcal{T}_k$ a family of manifolds $\{\Gamma_\delta\}_{0 \leqslant \delta \leqslant 1}$ by translating Γ along the diagonal (h, h, h); that is, $\Gamma_\delta = \Gamma + \delta(h, h, h)$ with $\delta \in [0, 1]$. For the surface example, we compute the condition number $\kappa_\delta(\mathcal{A})$ for $\delta = l/500$, $l = 0, \dots, 500$, as the ratio of the absolute value of the largest (in modulus) and smallest (in modulus), non-zero eigenvalue. For the curve example, a higher sampling rate defined by $\delta = l/10000$, $l = 0, \dots, 10000$ is used to reveal the high number of strong peaks in the condition number plots for the unstabilized method. To study the h dependency of the condition number, the minimum, maximum, and the arithmetic mean of the scaled condition numbers $h^2\kappa_\delta(A)$ are computed for each mesh size h. The resulting numbers displayed in Table 3 confirm the $O(h^{-2})$ bound proven in Theorem 4.2.

h	$\min_\delta\{h^2\kappa_\delta(\mathcal{A})\}$	$\max_\delta\{h^2\kappa_\delta(\mathcal{A})\}$	$\text{mean}_\delta\{h^2\kappa_\delta(\mathcal{A})\}$
$1.00{\cdot}10^{-1}$	1.41	2.14	1.75
$6.67{\cdot}10^{-2}$	1.29	2.03	1.59
$5.00{\cdot}10^{-2}$	1.26	1.79	1.53
$3.33{\cdot}10^{-2}$	1.25	1.67	1.46
$2.50{\cdot}10^{-2}$	1.22	1.60	1.45
$1.67{\cdot}10^{-2}$	1.22	1.57	1.46

(A) Translated surface example computed with bilinear form $a_h^2(v, w) + \tau s_h^3(v, w)$

h	$\min_\delta\{h^2\kappa_\delta(\mathcal{A})\}$	$\max_\delta\{h^2\kappa_\delta(\mathcal{A})\}$	$\text{mean}_\delta\{h^2\kappa_\delta(\mathcal{A})\}$
$1.00{\cdot}10^{-1}$	6.11	7.76	6.87
$6.67{\cdot}10^{-2}$	6.56	8.13	7.11
$5.00{\cdot}10^{-2}$	6.91	7.81	7.41
$3.33{\cdot}10^{-2}$	7.86	8.44	8.12
$2.50{\cdot}10^{-2}$	7.64	8.64	7.89
$1.67{\cdot}10^{-2}$	7.89	8.76	8.09

(B) Translated curve example computed with bilinear form $a_h^2(v, w) + \tau s_h^2(v, w)$

TABLE 3. Minimum, maximum, and arithmetic mean of the scaled condition number for various mesh sizes h.

In Figure 5, the condition numbers computed on $\mathcal{T}_2$ are plotted as a function of the position parameter delta. For the surface example, different stabilization parameters τ for the normal-gradient stabilization are tested and the resulting plots show clearly that the computed condition numbers are robust with respect to the translation parameter δ when τ is chosen large enough, i.e. $\tau \sim 1$. In contrast, the condition number is highly sensitive and exhibits high peaks as a function of δ if we set the penalty parameter τ to 0. Note that for very large parameters, the size of the condition numbers, while robust with respect to δ, increases again. For the curve example, we observe a similiar, albeit more extreme behavior as the condition number distribution shows more frequent and stronger peaks in the unstabilized case. Here, the full gradient stabilization $s_h^2(v, w)$ was employed. An additional τ parameter study gave very similar results to the studies

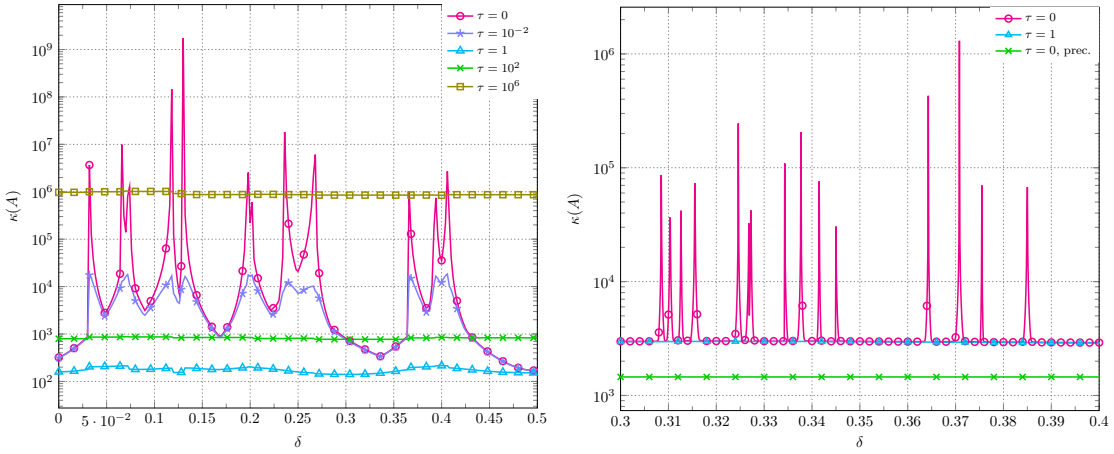

FIGURE 5. Condition numbers plotted as a function of the position parameter δ for different stabilizations and penalty parameters. (Left) Surface example where a combination of the full gradient form $a_h^2(v,w)$ and the normal gradient stabilization $s_h^3(v,w)$ was used. (Right) Curve example, with a combination of the full gradient form $a_h^2(v,w)$ and the full gradient stabilization $s_h^2(v,w)$. As the peaks in the 1-d curve example are more frequent and more pronounced, a narrower x-axis range was chosen. Both stabilization and diagonal preconditioning yield discrete systems with geometrically robust condition numbers.

performed in [7] for full gradient stabilized surface PDE methods, and thus is not included here. In particular, we observed that the condition numbers do not increase again for excessively high choices of τ.

Finally, we conduct a last numerical experiment inspired by the results presented in [26, 31]. In [31] it was proven that diagonal preconditioning yields robust condition number bounds and cures the discrete system from being severely ill-conditioned when a continuous piecewise linear ansatz space is used in combination with the full gradient form a_h^2. While the analysis provided in [31] considered only the codimension $c = 1$ case, our numerical experiments with the curve example indicate that this conclusion remains valid in the case $c > 1$, see Figure 5 (right).

ACKNOWLEDGEMENTS

This research was supported in part by EPSRC, UK, Grant No. EP/J002313/1, the Swedish Foundation for Strategic Research Grant No. AM13-0029, the Swedish Research Council Grants Nos. 2011-4992, 2013-4708, and Swedish strategic research programme eSSENCE.

REFERENCES

[1] G. E. Bredon. *Topology and geometry*, volume 139. Springer Science & Business Media, 1993.
[2] E. Burman. Ghost penalty. *Comptes Rendus Mathematique*, 348(21-22):1217–1220, 2010.
[3] E. Burman, S. Claus, P. Hansbo, M. G. Larson, and A. Massing. CutFEM: discretizing geometry and partial differential equations. *Internat. J. Numer. Meth. Engrg*, 104(7):472–501, November 2015.
[4] E. Burman, P. Hansbo, and M. G. Larson. A stabilized cut finite element method for partial differential equations on surfaces: The Laplace–Beltrami operator. *Comput. Methods Appl. Mech. Engrg.*, 285:188–207, 2015.
[5] E. Burman, P. Hansbo, M. G. Larson, and S. Zahedi. Stabilized CutFEM for the convection problem on surfaces. *arXiv preprint arXiv:1511.02340*, pages 1–32, 2015.
[6] E. Burman, P. Hansbo, M. G. Larson, and A. Massing. A cut discontinuous Galerkin method for the Laplace–Beltrami operator. *IMA J. Numer. Anal.*, 37(1):138–169, 2016. doi: 10.1093/imanum/drv068.

[7] E. Burman, P. Hansbo, M. G. Larson, A. Massing, and S. Zahedi. Full gradient stabilized cut finite element methods for surface partial differential equations. *Comput. Methods Appl. Mech. Engrg.*, 310:278–296, October 2016. ISSN 0045-7825. doi: http://dx.doi.org/10.1016/j.cma.2016.06.033. URL http://www.sciencedirect.com/science/article/pii/S0045782516306703.

[8] E. Burman, P. Hansbo, M.G. Larson, and S. Zahedi. Cut finite element methods for coupled bulk-surface problems. *Numer. Math.*, 133:203–231, 2016.

[9] A. Y. Chernyshenko and M. A. Olshanskii. An adaptive octree finite element method for pdes posed on surfaces. *Comput. Methods Appl. Mech. Engrg.*, 291:146–172, 2015.

[10] K. Deckelnick, C. M. Elliott, and T. Ranner. Unfitted finite element methods using bulk meshes for surface partial differential equations. *SIAM J. Numer. Anal.*, 52(4):2137–2162, 2014.

[11] A. Demlow. Higher-order finite element methods and pointwise error estimates for elliptic problems on surfaces. *SIAM Journal on Numerical Analysis*, 47(2):805–827, 2009.

[12] A. Demlow and G. Dziuk. An adaptive finite element method for the Laplace-Beltrami operator on implicitly defined surfaces. *SIAM Journal on Numerical Analysis*, 45(1):421–442, 2007.

[13] A. Demlow and M. A. Olshanskii. An adaptive surface finite element method based on volume meshes. *SIAM J. Numer. Anal.*, 50(3):1624–1647, 2012.

[14] G. Dziuk. Finite elements for the Beltrami operator on arbitrary surfaces. In *Partial differential equations and calculus of variations*, volume 1357 of *Lecture Notes in Math.*, pages 142–155. Springer, Berlin, 1988.

[15] G. Dziuk and C. M. Elliott. Finite element methods for surface PDEs. *Acta Numer.*, 22: 289–396, 2013.

[16] A. Ern and J.-L. Guermond. Evaluation of the condition number in linear systems arising in finite element approximations. *ESAIM: Math. Model. Num. Anal.*, 40(1):29–48, 2006.

[17] J. Grande and A. Reusken. A higher order finite element method for partial differential equations on surfaces. *SIAM Journal on Numerical Analysis*, 54(1):388–414, 2016.

[18] J. Grande, C. Lehrenfeld, and A. Reusken. Analysis of a high order Trace Finite Element Method for PDEs on level set surfaces. *ArXiv e-prints*, November 2016.

[19] A. Gray. *Tubes*, volume 221. Birkhäuser, 2012.

[20] P. Grisvard. *Elliptic problems in nonsmooth domains*, volume 24 of *Monographs and Studies in Mathematics*. Pitman Advanced Publishing Program), Boston, MA, 1985.

[21] S. Groß, M. A. Olshanskii, and A. Reusken. A trace finite element method for a class of coupled bulk-interface transport problems. *ESAIM: Math. Model. Numer. Anal.*, 49(5):1303–1330, Sept. 2015. doi: 10.1051/m2an/2015013.

[22] A. Hansbo, P. Hansbo, and M. G. Larson. A finite element method on composite grids based on Nitsche's method. *ESAIM: Math. Model. Num. Anal.*, 37(3):495–514, 2003.

[23] P. Hansbo, M. G. Larson, and S. Zahedi. Characteristic cut finite element methods for convection–diffusion problems on time dependent surfaces. *Comput. Methods Appl. Mech. Engrg.*, 293:431–461, 2015.

[24] P. Hansbo, M.G. Larson, and A. Massing. A stabilized cut finite element method for the Darcy problem on surfaces. *Comput. Methods Appl. Mech. Engrg.*, 326:298 – 318, 2017. ISSN 0045-7825. doi: https://doi.org/10.1016/j.cma.2017.08.007. URL http://www.sciencedirect.com/science/article/pii/S0045782517301548.

[25] M. G. Larson and S. Zahedi. Stabilization of Higher Order Cut Finite Element Methods on Surfaces. *ArXiv e-prints*, October 2017.

[26] M. A. Olshanskii and A. Reusken. A finite element method for surface PDEs: matrix properties. *Numer. Math.*, 114(3):491–520, 2010.

[27] M. A. Olshanskii and A. Reusken. Error analysis of a space-time finite element method for solving PDEs on evolving surfaces. *SIAM J. Numer. Anal.*, 52(4):2092–2120, 2014.

[28] M. A. Olshanskii, A. Reusken, and J. Grande. A finite element method for elliptic equations on surfaces. *SIAM J. Numer. Anal.*, 47(5):3339–3358, 2009.

[29] M. A. Olshanskii, A. Reusken, and X. Xu. A stabilized finite element method for advection–diffusion equations on surfaces. *IMA J. Numer. Anal.*, 34(2):732–758, 2014.
[30] M. A. Olshanskii, A. Reusken, and X. Xu. An Eulerian space-time finite element method for diffusion problems on evolving surfaces. *SIAM J. Numer. Anal.*, 52(3):1354–1377, 2014.
[31] A. Reusken. Analysis of trace finite element methods for surface partial differential equations. *IMA J. Numer. Anal.*, 35:1568–1590, 2014.
[32] H. Weyl. On the volume of tubes. *American Journal of Mathematics*, 61(2):461–472, 1939.

(Erik Burman) Department of Mathematics, University College London, London, UK–WC1E 6BT, United Kingdom
E-mail address: e.burman@ucl.ac.uk

(Peter Hansbo) Department of Mechanical Engineering, Jönköping University, SE-55111 Jönköping, Sweden.
E-mail address: peter.hansbo@ju.se

(Mats G. Larson, André Massing) Department of Mathematics and Mathematical Statistics, Umeå University, SE-90187 Umeå, Sweden
E-mail address: mats.larson@umu.se
E-mail address: andre.massing@umu.se